Three-dimensional imaging of garnet porphyroblast sizes and chemical zoning: Nucleation and growth history in the garnet zone

Frank S. Spear and Christopher G. Daniel

Department of Earth and Environmental Sciences, Rensselaer Polytechnic Institute,
Troy, New York 12180 <spearf@rpi.edu>
(Received July 1, 1998; Published October 30, 1998)

Abstract

The three-dimensional (3-D) growth history of two garnet zone samples (Grt + Chl + Bt + Ms + Pl + Qtz + Ilm) from southwestern Maine was examined by serial sectioning and 3-D reconstructions of compositional zoning from backscatter images and X-ray maps.

Mn, Fe, Mg, and Ca zoning is broadly concentric. The concentration of Mn in garnet cores generally correlates with size (d = 50 to 750 microns), indicating progressive nucleation. In detail, all elements show irregular, patchy zoning in the cores. Assuming constancy of Mn on the rims of all garnet crystals in a rock volume plus no subsequent diffusional modification, Mn concentration can be used as a "time line" for garnet growth. Examination of the evolution of individual garnet crystals reveals that multiple nuclei formed simultaneously in the core regions and that nuclei expanded by growth in amoeba-shape forms along preexisting mineral grain boundaries (primarily quartz and plagioclase), dissolving the interior grains until the grains were either gone or encapsulated, at which time dissolution ceased. Amoeba-shaped garnet crystals coalesced as they grew and, simultaneously, new nuclei appeared in the nearby matrix. The net result was a single garnet porphyroblast that formed by the growth and coalescence of multiple nuclei.

Radius-rate plots, constructed by counting pixels in 2-D images, reveal that crystals grew at the same radial rate, regardless of size. The observation of continuous nucleation in the vicinity of preexisting crystals plus the radius-rate plots rule out diffusion over length scales on the order of the garnet radius or greater as the rate-limiting step and are consistent with either diffusion over shorter length scales or interface control as rate-limiting to garnet growth. The strong clustering of garnet nuclei requires clustering of favorable nucleation sites, which may have been caused by favorable orientation of garnet precursor minerals (i.e. chlorite + quartz).

Keywords: kinetics, nucleation, growth, garnet

Introduction

Rates of metamorphic recrystallization (i. e. nucleation and mineral growth), when coupled with knowledge of metamorphic P-T histories, have the potential of providing important constraints on rates of crustal heating, loading, uplift, and cooling during orogenesis, and consequently, on the rates of tectonic processes. Although considerable advances have been made

in the development of kinetic theory (e.g. Lasaga and Kirkpatrick, 1981; Kerrick et al., 1991; Joesten, 1991), rates of nucleation and crystal growth in metamorphic rocks have traditionally been difficult to quantify.

This study was undertaken to obtain information on the three-dimensional spatial distribution and chemical zoning of garnet that could be used to evaluate models of garnet nucleation and subsequent growth and consumption. Although crystal size distribution data have been presented for garnet from a number of areas, and chemical zoning in garnet as a function of garnet size has been described (e.g., Jones and Galwey, 1966; Kretz, 1966, 1969, 1973, 1974, 1993; Finlay and Kerr, 1979, 1987; Cashman and Ferry, 1988; Carlson, 1989, 1991; Miyazaki, 1991; Carlson and Denison, 1992; Carlson et al., 1995; Denison and Carlson, 1997; Chernoff and Carlson, 1997) no systematic study of both crystal size distribution and chemical zoning as a function of metamorphic grade has ever been attempted. Additionally, only Chernoff and Carlson (1977) have reported a data set in which chemical zoning has been documented as a function of both garnet size and spatial position. These data are crucial for distinguishing among the several competing models of garnet growth. Garnet is arguably the most valuable mineral for providing constraints on the evolution of pressure and temperature conditions of metamorphism. The more that is known about the mechanisms of garnet nucleation and growth, the better constrained will be the petrologic models that utilize garnet.

This study includes data on samples that span the garnet, staurolite, and andalusite zones in order to examine processes of nucleation and growth from the first appearance of garnet near the garnet isograd through major garnet consuming reactions (the staurolite and andalusite isograds). This first paper presents results on two rocks from the garnet zone and will be followed by a companion paper on the higher grade rocks.

Geologic setting and petrography of the samples

The samples chosen for study come from a well-exposed section of metamorphic rocks in the Casco Bay area, southwestern Maine that span the garnet, staurolite, and andalusite zones (Hussey, 1988; Lang and Dunn, 1990; Grover and Lang, 1995). The area is characterized by low-pressure, Buchan type metamorphism at a pressure of 2-3 kbar (Grover and Lang, 1995).

Garnet-grade samples come from a coastline outcrop of the Jewel Formation on the southeast tip of Harpswell Neck (stop 1 of Grover and Lang, 1995). The rocks are relatively fine-grained schists with the assemblage chlorite + biotite + muscovite + garnet + quartz + plagioclase + ilmenite + graphite (Figs. 1 and 2).

Matrix foliation is defined by muscovite, biotite, and chlorite. In sections cut perpendicular to foliation (Figs. 1 and 2), quartz-rich pressure shadows are observed at the margins of garnet porphyroblasts parallel to foliation. In sections cut parallel to foliation (Fig. 3), it is confirmed that the pressure shadows are roughly circular in shape. In addition, many garnet pressure shadows also contain prismatic crystals of chlorite and biotite that radiate from the central garnet crystal (Fig. 3). These observations suggest flattening as the dominant deformation mechanism for formation of the matrix foliation. In addition, inclusions of quartz within garnet define a preexisting foliation at high angle to the matrix foliation (Figs. 1,2).

Geothermometry using garnet-biotite Fe-Mg exchange and the calibration of Ferry and Spear (1978) and Berman's (1990) solution model for garnet yields garnet rim + matrix biotite temperatures of 450-470 ˚C. Geobarometry using garnet + plagioclase + muscovite + biotite equilibria yields a pressure of 2-3 kbar at these temperatures.

Collection of three-dimensional composition data

Three-dimensional compositional data were obtained using the method of serial sectioning and electron microprobe mapping of each layer. Data analysis was performed on a Macintosh computer using the public domain NIH Image program (developed at the U.S. National Institutes of Health and available on the Internet at http://rsb.info.nih.gov/nih-image/; Rasband, 1997), Adobe Photoshop, and programs written in FORTRAN by the authors.

Layer spacing

A 3 cm diameter cylinder of rock was prepared from each sample, mounted on an aluminum plate for stability and strength and embedded in epoxy. Ten layers were analyzed on each section. The sample was ground to the desired thickness using 240 grit alumina grinding paper, polished, and the thickness measured with a micrometer to ±2 μm. The distances between layers are listed in Table 1. For the first six layers, the nominal distance between layers was 25 and 30 μm, respectively, for samples 96-1 and 96-2. However, it was determined that this was smaller than needed so the spacing was increased to 45 μm for the last three layers. Although measurement of the rock thickness was accurate, it was not always possible to achieve exactly the desired spacing between layers and the deviation from nominal spacing was approximately ±10 μm. It was also not possible to grind the sample perfectly parallel and thickness variations across the 3 cm sample were as large as ±20 μm. The lack of parallelism was inconsequential for this study, however, because composition data was collected on an area smaller than 0.6 cm^2 and the thickness was always measured over this same area.

From this work it was determined that the optimal spacing between layers is approximately 10% of the diameter of the largest garnet in the section, which provides ten layers of data to characterize the three-dimensional zoning of the largest garnet. This spacing yields fewer than 10 layers for smaller garnet crystals, but the zoning of smaller crystals tends to mimic only the outer shells of the larger crystals and is thus adequately characterized by fewer layers. In the samples studied here, the smallest garnet crystals observed were 15-20% of the diameter of the largest ones, ensuring that every garnet would be intersected by at least one section.

Layer registration

In order to reconstruct a three-dimensional image from 2-dimensional serial sections, it is necessary that each layer be registered with respect to other layers. For backscatter images and X-ray maps of the two garnet-zone samples, the layers were registered relative to the 5th layer. Rotation and translation was accomplished with the registration function in NIH image. More precise registration of individual garnet layers was accomplished with multiple layers in Adobe

Photoshop. Coarse registration was accomplished by aligning vertical copper wires that had been attached to the sample edge and embedded in epoxy. Final registration was achieved visually.

Backscatter electron mosaic images

Mosaics of backscatter electron images (BSE) were collected for each detailed analysis area on each layer using Program DPict from Geller Microanalytical, Peabody, MA. Each tile was scanned at 40x magnification (3.3 mm x 3.3 mm) with a spatial resolution of 5 μm/ pixel, sample current = 50 nA and a dwell time of 0.1 ms. The total area scanned was approximately 7 x 9 mm and 9 x 9 mm for samples 96-1 and 96-2 respectively. Representative BSE images from each sample are shown in Figures 4 and 5.

X-ray mapping

It was deemed impractical to collect X-ray maps of both garnet plus matrix for every layer, so it was necessary to write software that would collect X-ray maps and store the data in a manner that preserved the relative spatial position of each garnet. The program was written in Basic to run on Geller Microanalytical's Electron Microprobe Automation system. The user sets the registration point for the layer and then selects the corners of each individual garnet to be mapped. Data are stored as two-dimensional images at 16 bits/pixel with areas not analyzed set to black. To optimize data acquisition speed, data were collected by setting the microprobe stage in motion at a constant velocity and collecting counts at a set interval (typically 20 ms) to yield a spatial resolution of approximately 5 μm/pixel. Each pixel therefore represents the average counts collected over the 5 μm distance the stage traveled as counts were collected. Sample current was 300 nA at 15 kV accelerating voltage.

Secondary standards were mapped before and after each layer using identical operating conditions. The average pixel value of the standard maps was calculated and normalized to the nominal standard composition, and the garnet maps from each layer corrected by the same factor to yield semi-quantitative composition maps. Standards used were Gore Mountain garnet for Mg, Ca, and Fe, and Betts rhodonite for Mn. X-ray maps were further filtered by rendering black those pixels that were not garnet.

Approximately 30 garnet crystals were mapped on each layer for the elements Na, Ca, Mg, Fe, and Mn. Total analysis time/layer was 4-6 hours and the image for each layer requires 3-5 Mb of storage per element for a total storage requirement per layer of 20-30 Mb. The centers of 59 crystals in 96-1 and 44 crystals in 96-2 were intersected and analyzed. Representative Mn X-ray maps of a single layer for each sample are shown in Figures 4 and 5. The layers were assembled into stacks using NIH Image and the largest diameter selected for each garnet and copied into composite images for radius-rate and nucleation studies (Fig. 6). The locations and sizes of garnet crystals in part of each sample are viewed in a three-dimensional representation in Figure 7.

Image processing

Values of individual pixels in X-ray composition maps are imprecise, because the large number of pixels counted require short counting times/pixel. For example, absolute counts on Mn from

sample 96-1 range from 275 (core) to 85 (rim) resulting in √N counting statistics of 6% and 11%, respectively. Smoothing (averaging) kernels replace the center pixel in an nxn array of pixels (where n is odd) by the average of the n^2 pixels. When applied to X-ray maps, this standard procedure has the unfortunate property of blurring boundaries between garnet and inclusions or matrix. To circumvent this, we developed an algorithm that applies a smoothing kernel with edge/inclusion recognition. The garnet composition window is defined and only pixels within that window are used in the average for every kernel. Center pixels that fall outside the window are not changed. Experimentation with kernels ranging in size from 3x3 to 15x15 revealed that for the images collected here, a 7x7 smoothing kernel provided ample noise reduction without obliterating features of interest. The smoothing algorithm was applied using FORTRAN code written by the authors.

A major advantage of applying a smoothing kernel is the reduction of the apparent statistical error on each pixel, which simplifies the measurement of area using NIH Image. The smoothing kernel reduces the error on each pixel by 1/n where n is the dimension of the kernel by trading off analytical uncertainty for spatial resolution. For example, application of a 7x7 smoothing kernel to the Mn images collected in this study reduced the relative error from 6 to 0.9 % (core) and 11 to 1.6 % (rim), respectively. This corresponds to an absolute error in MnO concentration of approximately 0.2 wt. % (core) and 0.13 wt. % (rim).

Results

Several gigabytes of data were generated in the course of this study and it is not possible to show all data here. Moreover, the X-ray composition maps are best viewed interactively in color using a program such as NIH Image with layers assembled as stacks so differences between layers can be readily compared.

Chemical zoning

Garnet zoning is broadly concentric for Mn, Fe, Mg, and Ca (Fig. 8; Table 2). The most striking feature of these garnet crystals is the high Mn concentrations, which have core-to-rim variations of 20.5 to 8 weight per cent (47-18 mole percent) (see also Grover and Lang, 1995). Fe and Mg increase from core to rim whereas Ca increases from low values in the core to the highest values near the rim before dropping off to the lowest values at the rim.

The zonation of Fe, Mg, and Mn are strongly correlated. In contrast, Ca zoning does not mimic Fe, Mn, and Mg zoning exactly. This can be seen in Figure 8a where Ca zoning is radially symmetric whereas Mn (or Fe and Mg) zoning shows two regions of high (or low) concentration in the upper right and left sides of the crystal. This observation suggests that Mn, Fe, and Mg behave similarly with respect to the degree of local equilibration whereas Ca behaves independently, as also found by Chernoff and Carlson (1997).

Although the zoning in all elements is broadly concentric, detailed examination reveals a more complex pattern. It is apparent from examination of the numerous X-ray maps that many garnet crystals are actually composed of more than one crystal that have coalesced during growth. An excellent example is seen just below and to the left of garnet 1 in sample 96-1 (Fig. 4). Indeed,

garnet 1 itself (Fig. 8a) is clearly composed of two individual parts (upper right and lower left) that have grown together to form a single crystal.

Garnet nucleation and growth

Application of the 7x7 smoothing kernel (Fig. 9) reveals that Mn is not concentric about individual parts of the garnet, but rather is zoned in irregular, amoeba-like shapes, a pattern that reflects fast growth along grain boundary surfaces and slower dissolution and replacement of quartz inclusions.

Many workers (e.g. Kretz, 1973, 1974; Carlson, 1989, 1991; Denison and Carlson, 1997) have assumed that the composition of Mn, Fe, and Mg is the same on the rims of all garnet crystals in a sample at an instant in time and Chernoff and Carlson (1997) present compelling evidence in support of this hypothesis. That is, local equilibrium is maintained for these elements throughout the volume of a hand sample. If subsequent diffusion does not modify the growth profiles, the zoning in these elements serves as a "time line" and can be used to illustrate the history of garnet growth.

The strong correlation observed among the detailed zoning of Fe, Mg, and Mn supports the hypothesis that these elements achieved a close approach to local equilibrium during garnet growth. Additional support comes from the observation that Fe/(Fe+Mg) correlates positively with Mn content (Fig. 8). If variations of Mn, Fe, and Mg were due solely to local variations in bulk composition then mass balance and phase equilibrium considerations would predict antithetic zoning of Fe, Mg, and Fe/(Fe+Mg) with respect to Mn. That is, if local equilibrium among these elements on the scale of a thin section were not achieved and the zoning observed was due differences in bulk composition, then Fe/(Fe+Mg) should *decrease* with increasing Mn content. The opposite is observed (i.e. high Mn correlates with high Fe/(Fe+Mg). This requires that areas of high Mn formed at lower temperature, consistent with the hypothesis that Mn zoning can be used as a time line in these rocks.

Figure 10 shows the evolution of garnet growth using Mn zoning as a "time line". As seen in Figure 10a (cumulative garnet growth), two isolated patches of garnet appeared first, with each composed of more than a single nucleus (frame 17.5). With growth, these nuclei expanded and eventually coalesced. The shapes of the growth patterns of expanding nuclei suggest they grew along preexisting grain boundaries, dissolving the foreign material (mostly quartz). New garnet surrounded foreign minerals until either the mineral was completely dissolved away, or the mineral was completely encapsulated in garnet (no longer in communication with the matrix). An especially good example of the dissolution of a quartz crystal that was arrested before completion is seen in the upper right part of the crystal starting with frame 16. In frame 16, garnet begins to surround two quartz inclusions and a new nucleus appears directly below the two quartz grains. In frame 15, one quartz crystal is completely surrounded by garnet and the other is nearly surrounded. In frame 14, both quartz grains are completely surrounded by garnet. The quartz grain on the lower right was isolated from the matrix because no further dissolution of quartz or garnet growth is observed in the vicinity. The quartz grain to the upper left continued to dissolve and be replaced by garnet through frame 12 where it, too, became isolated from the matrix. Many examples of this type of

growth behavior can be seen and, indeed, it appears to characterize the way in which garnet grew in these samples.

Equally important, as the garnet grew, new nuclei continuously appeared. Some of these new nuclei are relatively close to the boundary of existing garnet, for example, in frame 17.5 and 17. However, often the new nuclei appeared relatively far (e.g. 150 μm) from existing garnet (e.g. frame 14). Figure 11 shows the distribution of distinct nuclei observed in this garnet slice. Most are concentrated in the central part of the garnet, suggesting a localized affinity for garnet nucleation. Growth of the central garnet core therefore proceeded dominantly by continuous formation of new nuclei, growth of existing nuclei, and coalescence of growing crystals. The outer margin of garnet appears to have formed dominantly by growth on existing material.

Nucleation rate was examined by selecting a window of MnO concentration using the "threshold" option in NIH Image and counting new nuclei as a function of MnO concentration (Fig. 12). Distinguishing a new nucleus from statistical noise was made using two criteria: (1) The new nucleus must be greater than 5 pixels (25 μm) from existing garnet; and (2) The new nucleus must be separated from existing garnet by a compositional valley greater than 0.5 weight %. The distance of 25 μm for the first criterion was chosen based on analysis of synthetic zoning images using counting statistics similar to those of the natural samples and processed in the identical manner. It was observed in these synthetic images that, although new nuclei could be generated from statistical noise, they were always within 1-3 pixels of the existing garnet. The value of 0.5 weight per cent used in the second criterion was chosen to be $> 2\sigma$ of the counting statistics of individual pixels in the smoothed image. By requiring that there be a compositional valley $>2\sigma$ between the new nucleus and existing garnet ensures the compositional island represented by the nucleus is statistically significant. These criteria are fairly stringent and in practice approximately 10% of observed isolated Mn pixels were rejected. It should be emphasized, however, that these criteria are applied in two-dimensional images. Some apparent nuclei may connect to preexisting garnet in the third dimension, although examination of selected garnet crystals in 3-dimensions (e.g. Fig. 16b) indicates that most of the nuclei are not connected in the third dimension.

Using these criteria, new nuclei were counted and plotted as a function of MnO concentration and the number of nuclei normalized to the volume of rock examined (Fig. 12). Sample 96-2 contains garnet crystals with the highest core MnO concentrations, and presumably began to nucleate garnet earliest. The two outliers on the plot for sample 96-2 at 27 and 28 wt. % MnO are from two garnet crystals that have anomalously high MnO concentrations in localized domains near their cores (Fig 13). These high-Mn anomalies are interpreted as detrital and signify that localized high-Mn regions may have existed in the samples prior to the main phase of garnet nucleation and growth. Nucleation of new garnet in sample 96-2 began at 21 wt. % and increased to a maximum at approximately 19 wt. %, then decreased gradually until nucleation ceased at approximately 8 wt. %. Sample 96-1 began nucleation at approximately 18 wt. % and the nucleation rate increased rapidly to values similar to sample 96-2. Inasmuch as both samples contain abundant chlorite, it is concluded that the cessation of nucleation at approximately 8.0 wt. % MnO corresponds to the metamorphic peak, and not a loss of reactants.

Both samples display similar nucleation histories, with the exception that sample 96-2 displays a stage of rapid nucleation from 20-18 wt. %, before sample 96-1 began to nucleate garnet. It is

suggested that the rapid nucleation rate recorded by sample 96-2 reflects a phase of rapid heating. This rapid heating was felt by both samples (they were collected less than a meter from one another), but was recorded only in sample 96-2 because of its higher bulk MnO content. The similarity between samples observed in Figure 12 suggests that nucleation rate calculated in this manner may be a means to estimate relative heating rates in different terranes.

Radius-rate calculations

General considerations

Radius-rate relations, defined by plots of normalized radius ($c = r_i/r_{max}$) versus normalized rate ($C = \Delta r_i/\Delta r_{max}$), where the subscript "i" refers to the garnet of interest and the subscript "max" refers to the largest garnet in the sample, have been used to evaluate the relative rates of growth of garnet crystals of different size (Kretz, 1974; Carlson, 1989, 1991; Denison and Carlson, 1997). As developed by Kretz (1974), three end-member models can be envisioned:

Case 1: Radial growth rate is a constant: $dr/dt = k_1$.
Case 2: Area growth rate is constant: $da/dt = k_2$; $dr/dt = k_2/8\pi r$.
Case 3: Volumetric growth rate is constant: $dv/dt = k_3$; $dr/dt = k_3/\pi r^2$.

Extending this treatment, Carlson (1989) developed equations to predict radius- rate relations assuming thermally accelerated diffusional growth (Case 2a).

Each model predicts different growth behavior for individual crystals as a function of time (Fig. 14a). In addition, each model predicts different behavior for crystals of different sizes for a specific growth (i.e. time) increment, as shown on the normalized radius-rate plot (Fig. 14b). For Case 1, garnet crystals of all sizes grow at the same radial rate, so $\Delta r_i/\Delta r_{max} = 1$. For Cases 2 and 3, the radial rate of garnet growth is a function of the garnet size: Case 2: $\Delta r_i/\Delta r_{max} = 1/(r_i/r_{max})$; Case 3: $\Delta r_i/\Delta r_{max} = 1/(r_i/r_{max})^2$. For both cases 2 and 3, small crystals grow faster than large crystals. Carlson's (1989) model (Case 2a) is represented by three curves representing three crystals nucleated at different times (τ) relative to the largest garnet. The critical feature of the radius-rate plot for this model is that it dips below values of 1.0 ($\Delta r_i/\Delta r_{max} < 1.0$) at large values of r_i/r_{max}. When $\Delta r_i/\Delta r_{max} < 1.0$, small crystals grow more slowly than large crystals.

To better visualize the types of Mn zoning to be expected in garnet from the three limiting cases of garnet growth, simulations similar to those described by Spear et al. (1990) were performed using a routine written for program Gibbs (Spear and Menard, 1989). The model assemblage included garnet + chlorite + biotite + muscovite + quartz + H_2O in the system SiO_2-Al_2O_3-MgO-FeO-MnO-K_2O-H_2O (MnKFMASH). Starting conditions were 500 ˚C, 5 kbar and additional simulation parameters are given in Table 3. Each simulation was run from 500 ˚C to 560 ˚C at constant pressure using temperature increments of 0.5 ˚C. The simulations began with one garnet/cm^3 and a new garnet was added to the rock volume after every 5.0 ˚C interval up to 525 ˚C for a final nucleation density of six garnet crystals/cm^3. At each 0.5 ˚C temperature increment, the equilibrium compositions of all phases were computed, and the incremental change in total garnet volume was computed from mass balance. This new volume was then distributed onto the surfaces of the existing garnet crystals within the representative 1 cm^3 volume using the geometric

constraints implied by Cases 1-3 (equal radial, area and volume increments), in the following manner.

Distribution of new garnet onto existing crystals is simple for Case 3 because each garnet receives the same volume, so the incremental volume added to each garnet is $\Delta V_i = \Delta V_{total}/(\text{number of crystals})$ where ΔV_{total} is the total volume of garnet produced during the current temperature increment. Because

$$\Delta V_i = \frac{4\pi}{3}(r_{i+1}^3 - r_i^3) \quad (1)$$

the new radius of each garnet is then

$$r_{i+1} = \left[\frac{3}{4\pi}(\Delta V_i + r_i^3)\right]^{1/3} \quad (2)$$

Case 2 requires distribution of the incremental volume of garnet onto existing garnet such that the area added to each garnet is identical, with the constraint that the total volume of garnet added is that produced over the temperature interval. The incremental area added to each garnet is

$$\Delta a = a_{i+1} - a_i = 4\pi(r_{i+1}^2 - r_i^2) \quad (3)$$

from which the new radius of each can be derived:

$$r_{i+1} = \sqrt{\Delta a/4\pi + r_i^2} \quad (4)$$

There is one such equation for each garnet in the sample volume. The total volume of garnet produced in the temperature interval is

$$\Delta V_{total} = \sum \frac{4\pi}{3}\left(r_{i+1}^3 - r_i^3\right) = \sum \frac{4\pi}{3}\left(\left(\frac{\Delta a}{4\pi} + r_i^2\right)^{3/2} - r_i^3\right) \quad (5)$$

which is a non-linear equation that was solved for Δa using Newton's method. Once Δa is known, the new radius of each garnet is computed from equation (4).

Case 1 requires distribution of the incremental volume of garnet onto existing garnet such that the radius added to each garnet (Δr) is identical, again with the constraint that the total volume of garnet added is that produced over the temperature interval. The total volume of garnet may be written

$$\Delta V_{total} = \sum \Delta V_i = \sum \frac{4\pi}{3}\left(r_{i+1}^3 - r_i^3\right) = \sum \frac{4\pi}{3}\left((r_i + \Delta r)^{3/2} - r_i^3\right) \quad (6)$$

which was rearranged into a cubic and solved for Δr.

Results of the simulations are shown in Figure 15. In each panel are shown Mn zoning profiles for six garnet crystals that nucleated at five degree intervals (500 – 525 ˚C). Also shown in each is a reference zoning profile (red) that represents the zoning that would be observed had only a single garnet nucleated. Profiles for the three cases show different slopes (Mn vs. radius). Profiles for Case I (equal radial increments; Fig. 15a) are gentlest and the profiles are parallel at all Mn concentrations, as required by the constraint of equal radial growth. Case 3 (equal volume increments) displays the steepest zoning towards the rim, and the zoning profiles for larger garnet crystals are steeper than those for smaller crystals. A particularly interesting feature of these simulations is the peaked core zoning predicted for Case 1, which follows from the equal radial growth constraint. Minor diffusion would quickly relax the peaks in the cores of the smaller crystals, so it is not likely that they would be preserved in medium to high-grade rocks.

Radius-rate plots such as Figure 14b using natural garnet data can, in principle, be used to determine which of the three models is applicable to a suite of garnet crystals. Case 1 has been attributed to isothermal interface-controlled growth, Case 2 and 2a to isothermal and thermally accelerated diffusion-controlled growth, respectively, and Case 3 to a heat-flow-controlled growth rate (Kretz, 1974; Carlson, 1989). However, we believe that heat-flow can only be (and most likely is in nearly all rocks) rate-limiting for the total volume of garnet growth, not for growth between competing crystals of different sizes, unless thermal gradients are present within an individual sample. Consequently, it is not clear that Case 3 has any true kinetic significance and should only be considered a geometric construct.

Application of the radius-rate relations requires correlating growth increments among all garnet crystals in a sample. Following Kretz (1973, 1974), workers have generally assumed that the composition of Mn, Fe, and Mg is the same on the rims of all crystals in a sample at an instant in time. Variations in Ca zoning as a function of garnet size suggest that this assumption is not valid in all cases for Ca (e.g. Carlson, 1989; Chernoff and Carlson, 1997). Incremental changes in Mn, Fe and Mg can then be correlated between crystals of different sizes to obtain radial growth changes as a function of time and size. As discussed by Carlson (1989), the consistency of radius-rate relations observed in Mn, Fe, and Mg suggests that this assumption is reasonable.

Kretz (1974) and Carlson (1989) applied this method in slightly different ways. Kretz plotted a single growth increment for garnet crystals of different sizes and thus obtained a snapshot of growth mechanisms at an instant in time where it could be assumed that the temperature was the same for all crystals. In contrast, Carlson plotted all growth increments (core to rim) for a single garnet pair and thus showed the overall growth history as presumably temperature, pressure, and perhaps mineral reaction changed. Kretz (1974) examined only FeO for his radius-rate measurements whereas Carlson used MnO, FeO, and MgO. In this study, we focus only on MnO inasmuch as it shows the largest core-to-rim variation, although preliminary results on FeO and MgO indicate that similar results would be obtained from these.

Technique for measuring area as a function of concentration

The present data set provides the opportunity to compare three different methods of calculating radius-rate relations. Previous studies plotted radial zoning profiles and measured radius and Δradius from these. This approach has the inherent uncertainty that the measured radial profile may

not be representative of the growth history, if the growth is not perfectly radially symmetric. A more accurate measure of the rate of garnet growth is to measure the area or the volume of garnet for a specified change in Mn, Fe or Mg.

Areas were measured on X-ray maps using NIH Image. First, the desired MnO window was set using a macro that converts the MnO concentration into pixel values (based on the standard values obtained at analysis time). A value of ΔMnO = 0.5 weight per cent was chosen for the window because this value is greater than 2σ of the counting statistics error on a single pixel in the smoothed images (7x7 kernel), ensuring the statistical significance of the measurements. The macro then set the "threshold" option to highlight this range in all maps. The desired threshold area in the garnet of interest was selected using the wand tool and the total number of pixels outlined by the wand tool was obtained using the "measure" command. The results were copied to a spreadsheet where areas were converted into radius assuming circular geometry. The change in radius between the outer and inner shell of the MnO window was then calculated by difference. Volumes were measured by summing areas in successive layers, multiplied by distances between layers. Although the number of layers examined in this study (ten) was insufficient to obtain three-dimensional zoning information on the largest garnet crystals in the sample (750 μm diameter), several intermediate size crystals were sampled in their entirety.

Results comparing methods

Figure 16 shows X-ray maps for all eight layers of a single garnet from sample 96-1 (garnet 22). The crystal is roughly euhedral in outline and multiple nuclei are readily observed in several layers. Growth of this garnet was typical of crystals from these samples, and the complexity of the growth history can be seen in 3-dimensions in Figure 16b. Nucleation was progressive, as evidenced by isolated bits of garnet away from the central crystal. Of particular note are the large cavities (quartz inclusions) within the garnet that shrink and become surrounded with time.

The areas corresponding to Mn concentrations ranging from 18 to 8 weight per cent were measured in each layer and converted to an apparent circular radius for comparison. Volumes were computed by summing individual layer contributions multiplied by the distances between the midpoints of adjoining layers and converted into an apparent spherical radius. In addition, five line traverses were measured directly off of the X-ray maps on two layers (Fig. 16).

Comparison of the three methods of calculating the apparent radius of garnet as a function of MnO concentration are shown in Figure 17. All apparent zoning profiles obtained from measuring areas on each layer show systematic variation between core composition and radius, with the exception of layer 9 (Fig. 17a). Moreover, all show trends parallel to the apparent radial zoning calculated from summing the total volume of garnet over all layers, and the zoning calculated from the center layer (layer 6) is a very good match for the zoning calculated from the total volume. In contrast, the zoning obtained from the line traverses (Fig. 17b) are quite variable, depending on the direction of the traverse. Moreover, no traverse intersects the highest MnO concentration in the core, nor is there a monotonic decrease in Mn with distance, requiring considerable smoothing of data in order to construct radius-rate plots using line traverses.

Comparison of Figures 17 and 15 reveals that using area or total volume measurements (Fig. 17a), the zoning profiles are roughly parallel, similar to Case 1 (Fig. 15a). In contrast, depending on which profiles were used, the traverse data (Fig. 17b) could be used to support Cases 1, 2, 2a or 3. These results indicate that accurate measures of total garnet grown as a function of MnO concentration can be obtained from area measurements on two-dimensional X-ray maps on near-center cuts through these garnet crystals.

Mn radius-rate relations

There is a strong correlation between the MnO concentration in garnet cores and crystal size (Figs. 6 and 18), at least up to a size of 200 - 250 μm. Core compositions are constant for garnet crystals greater than 250 μm radius. The flat slope for large crystals is the consequence of coalescence of several nuclei to form a single crystal. The strong correlation for smaller crystals suggests progressive nucleation in a matrix undergoing depletion of MnO. Moreover, rims have identical compositions, supporting the contention that MnO is constant on the rims of all garnet crystals throughout garnet growth and can thus be used as a "time line".

The areas corresponding to ΔMnO = 0.5 wt. % "windows" were measured on each center cut (Fig. 6) of smoothed composition maps (7x7 kernel) using the method described above. It was discovered after initial measurements that it was not possible to consider every garnet shown in Figure 6 as a single crystal. For example, as shown in Figures 9 and 10, early in its growth history, this garnet was composed of several nuclei, all of which grew with time. If growth of these nuclei are summed to give the total growth of the entire crystal, the growth of individual nuclei is inaccurately measured. The method finally adopted was to measure each nucleus separately as long as it was separated by at least 5 pixels (25 μm) from other nuclei. When two or more nuclei coalesced into a single crystal, they were thereafter treated as a single grain. Thus, the number of garnet crystals in the sample was continuously changing with time as nuclei coalesced and new nuclei appeared.

Unnormalized plots (Fig. 19) were chosen over previously used normalized radius-rate plots (e.g. Fig. 14) for several reasons. Firstly, the observation that new garnet continuously nucleated within what later became a "single crystal" means that the largest crystal in the sample was not necessarily the largest crystal throughout the growth history. Moreover, when two or more nuclei coalesced the growth rate decreases solely because of the reduced surface area, introducing additional difficulties in interpretation if a crystal undergoing coalescence is used as the normalizing factor. Finally, choosing a single garnet from the sample as the normalization factor leaves no room for statistical and geological uncertainty (e.g. if the largest garnet is simply different from most of the others). If such a garnet is chosen for the normalization factor, then all plots and interpretations drawn from them are biased by this one crystal. By plotting the unnormalized data, the trends exhibited by all crystals can be viewed without this bias. The appearance of normalized plots can be easily visualized from the plots in Figure 19 by scaling the axes by the value of r and Δr for the largest garnet in the plot. It should be noted again that in Figure 19, the radial change (Δr) is plotted against garnet radius (r) for a single composition interval (ΔMn), which is assumed to represent an interval in time. These plots are not directly equivalent to radius-rate plots presented by Carlson (1989), in which the normalized radial change ($\Delta r_i/\Delta r_{max}$) is plotted against normalized

radius (r_i/r_{max}) for a single pair of garnet crystals. Carlson's plots do not, therefore, represent a single time increment but rather the entire growth history of the smaller garnet.

The results presented in Figure 19 reveal radial changes that are broadly independent of garnet size (Case 1; Fig 14). For comparison, if small crystals grew faster (Case 2) or slower (Case 2a), the plots would show negative or positive correlations, respectively. Errors on measurement of radius are estimated to be approximately ± 1 pixel, or ± 5 μm, so the trends observed in the data lie within the error of measurement, although the scatter is larger for smaller crystals. One factor that would increase the measurement error is the measurement of multiple nuclei that have coalesced over a particular Mn interval as a single nucleus, which would result in measurement of a smaller radial change for a given garnet radius than isolated nuclei. Although attempts were made to avoid this problem, some of the scatter at small garnet radius is likely the result of this uncertainty. Additionally, measurement of the growth of small nuclei are likely to be more uncertain because uncertainties in measurement in the third dimension will more strongly influenced small crystals than large ones, which tend to grow more symmetrically.

Probably the largest source of scatter in Figure 19 stems from crystal shape (cf. Fig. 16b). Many crystals are not spherical but rather have amoeba-like shapes (although many crystals are approximately spherical for some intervals of their growth history). Evaluation of the effect of crystal shape on the radius-rate plots can be made in the following manner. Consider two crystals, one spherical and one amoeba-shaped. Both crystals will be assumed to have identical volumes so that both would have identical calculated radii assuming spherical geometry. Now add identical radial increments to each crystal. The sphere will incorporate a smaller volume than the amoeba-shaped crystal. Therefore, when the volume change (or area change in 2-D) is measured in each using the image processing techniques, the amoeba-shaped crystal will have a larger calculated Δr, even though both crystals had identical radial increments added to each. Test calculations using geometries similar to those observed in the suite of garnet crystals studied here reveal the variation in Δr may be as large as 50%. A better measure of incremental growth might be to measure the change in area (or volume) of garnet as a function of perimeter length (or surface area). Work towards this goal is in progress.

Interpretation of radius-rate data. Despite these uncertainties in the measurements, the radial change of garnet appears to be independent of garnet size. Compared with the three models presented earlier (Fig. 14), these observations are most consistent with the interpretation that rate-limiting step in garnet growth is interface processes. However, similar radius-rate relationships might be obtained from diffusion-controlled growth, provided the length scale for diffusion is small relative to the garnet radius.

It is possible to rule out the possibility that garnet growth was controlled by diffusion over length scales that are on the order of two or more garnet radii (Case 2). Even in the situation where the crystal shape deviates from spherical, if the diffusion field is large relative to the irregularities in the crystal shape, then spherical geometry will be a close approximation to the integrated flux at the surface. If crystals are well isolated, then a dependence of growth rate on crystal size with small crystals having grown faster than large crystals should be observed (a negative correlation in Fig. 19). However, in the samples studied here, nuclei are strongly clustered so that large diffusion fields would overlap substantially reducing the overall rate of growth for all clustered nuclei. The

data plotted in Figure 19 confirm that, within the error of measurement, there is no difference between the growth rate of isolated crystals that grew from single nuclei and the growth rate of crystals that grew in clusters.

However, if the diffusion field is small relative to either the matrix crystal size or the deviation of the garnet from spherical geometry, then diffusive control no longer predicts such a simple radius-rate relationship as was presented for Case 2 above. Consider, for example, the case where growth of garnet is perpendicular to a flat crystal face. One-dimensional diffusive flux to a flat crystal face is independent of the crystal size, so there should be no correlation between crystal size and growth rate. The radius-rate plot in this case would be identical to that for interface control (Case 1). It is difficult to evaluate exactly what the consequences of diffusive controlled growth on an amoeba-shaped crystal might be, but it is suspected that it would be intermediate between the two cases. A further complication arises when the length scale for diffusion becomes equivalent to or smaller than the matrix grain size. In this situation, significant diffusion must occur parallel to the garnet surface for growth to occur. This can readily be seen in Figure 10, in which the incremental growth of garnet is displayed. Where garnet grows around a quartz grain, Fe, Mg, Mn, Ca, and Al must be added and excess SiO_2 must be removed (by diffusion) from the interface in order for garnet to replace quartz. The existence of quartz inclusions proves that this process is not as efficient as overall garnet growth, suggesting diffusion control for at least one element.

In summary, the radius-rate data rule out diffusion over distances on the order of the garnet radius or larger as the rate-limiting step, but are consistent with either diffusion over shorter distances or surface process as rate limiting.

Discussion

The results presented in this paper differ significantly from those of Kretz (1973, 1974, 1993), Carlson (1989, 1991) and Denison and Carlson (1997), although direct comparison is difficult because of the different ways in which the data were collected. Kretz (1974, 1993) argued for interface control based on a small set of radius-rate data whereas Carlson (1989, 1991) and Denison and Carlson (1997) argued for diffusion control based on a much larger set of radius-rate data. Our data suggest that the rate-limiting step in garnet growth in these rocks is either interface-controlled or diffusion-controlled over length scales on the order of the average garnet radius or less. In addition, the pattern of nucleation, which exhibits strong clustering, virtually requires inhomogeneities in the sample that favor garnet nucleation in select regions.

The most surprising result of this study is the observation of continuous nucleation of garnet within a single garnet grain. An important question to ask is whether the separately nucleated regions of garnet are crystallographically distinct. We have examined the crystallographic orientation of single garnet grains using Scanning Electron Diffraction Microscopy at the University of Liverpool facility with the assistance of David Prior. Preliminary results indicate that there is no systematic correlation between garnet crystallographic orientation and nucleation site as evidenced by Mn zoning (Daniel and Spear, in preparation). That is, multiple-nuclei garnet grains are, in general, crystallographically continuous. The reason for this is not clear, but it is possible to rule out post-crystallization annealing because higher-grade garnet crystals, which presumably have a more favorable kinetic setting to promote annealing, sometimes display multiple

crystallographic orientations (Prior et al., 1998). The two remaining possibilities are (1) the separate garnet nuclei formed in similar crystallographic orientation or (2) Mn zoning does not, in fact, represent a time line and garnet grains did not grow with continuous nucleation.

The second possibility would require significant disequilibrium on a scale of 100-200 μm. That is, garnet growth would have to have occurred across locally different bulk compositions, adopting a composition appropriate for that bulk composition. As an example, the garnet illustrated in Figure 11 might have nucleated first with low Mn content, followed by sequential growth outwards towards the rim encompassing regions with higher Mn. However, as was mentioned earlier, phase equilibrium considerations dictate that Mn should correlate inversely with Fe/(Fe + Mg) if local bulk composition variations controlled garnet composition whereas Mn should correlate positively with Fe/(Fe + Mg) if progressive growth in a homogeneous bulk composition occurred. Inasmuch as a positive correlation is observed, it appears that disequilibrium at this scale is not a viable explanation.

The crystallographic homogeneity of garnet grains consisting of multiple nuclei (e.g. Fig. 11) requires, therefore, that all nuclei formed in similar orientation. The reason for this is not clear, but one possibility is that garnet formed on preexisting grains that shared a common orientation. The major garnet-producing reaction was chlorite + quartz = garnet + H_2O, and it is possible that individual garnet crystals nucleated on either a single chlorite crystal or on a cluster of chlorite crystals in similar orientation at sites where a chlorite + quartz grain boundary was favorably oriented. This was not strictly a pseudomorph reaction or epitaxial growth, but one that relied on preexisting crystallographic orientation of chlorite. This explanation might also explain the clustered nucleation pattern: chlorite crystals in certain orientations provided more favorable nucleation sites than others, so nucleation was favored on these crystals.

Whatever the explanation for the progressive, clustered nucleation of individual garnet grains, it is clear that nucleation sites were not homogeneously distributed throughout the sample volume. This implies that statistical studies of garnet spatial distribution and size (e.g. Kretz, 1969; Carlson, 1989; Denison and Carlson, 1997; Raeburn, 1996; Daniel and Spear, in press) may not reveal insights into growth processes (e.g. diffusion-controlled versus interface-controlled growth) but rather the heterogeneous distribution of garnet nucleation sites.

Acknowledgments

This work was supported by National Science Foundation grants EAR-9508104 and EAR-9805243 to FSS and a Rensselaer Graduate Fellowship to CGD. Careful and insightful reviews by A. Boyle and W. Carlson are gratefully acknowledged.

References cited

Berman, R.G. (1990) Mixing properties of Ca-Mg-Fe-Mn garnets. American Mineralogist, 75, 328-344.

Carlson, W.D. (1989) The significance of intergranular diffusion to the mechanisms and kinetics of porphyroblast crystallization. Contributions to Mineralogy and Petrology, 103, 1-24.

Carlson, W.D. (1991) Competitive diffusion-controlled growth of porphyroblasts. Mineralogical Magazine, 55, 317-330.

Carlson, W.D., and Denison, C. (1992) Mechanisms of porphyroblast crystallization: Results from high-resolution computed X-ray tomography. Science, 257, 1236-1239.

Carlson, W.D., Denison, C., and Ketcham, R.A. (1995) Controls on the nucleation and growth of porphyroblasts: kinetics from natural textures and numerical models. Geological Journal, 30, 207-225.

Cashman, K.V., and Ferry, J.M. (1988) Crystal size distribution (CDS) in rocks and the kinetics and dynamics of crystallization III. Metamorphic crystallization. Contributions to Mineralogy and Petrology, 99, 401-415.

Chernoff, C.B., and Carlson, W.D. (1997) Disequilibrium for Ca during growth of pelitic garnet. Journal of Metamorphic Geology, 15, 421-438.

Daniel, C.G., and Spear, F.S. (in press) Interface-controlled garnet growth in regional metamorphic rocks from Northwest Connecticut. Journal of Metamorphic Geology.

Denison, C., and Carlson, W.D. (1997) Three-dimensional quantitative textural analysis of metamorphic rocks using high-resolution computed X-ray tomography: Part II. Application to natural samples. Journal of Metamorphic Geology, 15, 45-57.

Ferry, J.M., and Spear, F.S. (1978) Experimental calibration of the partitioning of Fe and Mg between biotite and garnet. Contributions to Mineralogy and Petrology, 66, 113-117.

Finlay, C.A., and Kerr, A. (1979) Garnet growth in a metapelite from the Moinian rocks of Northern Sutherland, Scotland. Contributions to Mineralogy and Petrology, 71, 185-191.

Finlay, C.A., and Kerr, A. (1987) Evidence for differences in growth rate among garnets in pelitic schists from northern Sutherland, Scotland. Mineralogical Magazine, 51, 569-576.

Fisher, G.W. (1978) Rate laws in metamorphism. Geochimica et Cosmochimica Acta, 42, 1035-1080.

Grover, T., and Lang, H. (1995) Examination of a well-exposed sequence of garnet through sillimanite zone metapelitic rocks in Casco Bay. In A.M. Hussey, and R.A. Johnston, Ed., New England Intercollegiate Geological Conference Guidebook to Field Trips in Southern Maine and adjacent New Hampshire, p. 195-210. Bowdoin College, Brunswick, Maine.

Hodges, K.V., and Crowley, P.D. (1985) Error estimation and empirical geothermobarometry for pelitic systems. American Mineralogist, 70, 702-709.

Hussey, A.M., II (1988) Lithotectonic stratigraphy, deformation, plutonism and metamorphism, greater Casco Bay Region, southwestern Maine. In R.D. Tucker, and R.G. Marvinney, Ed., Studies in Maine Geology, 1, p. 17-34. Maine Geological Survey, Augusta, Maine.

Joesten, R.L. (1991) Kinetics of coarsening and diffusion-controlled mineral growth. In D.M. Kerrick, Ed., Contact Metamorphism, 26, p. 507-582. Mineralogical Society of America, Washington, D. C.

Jones, K.A., and Galwey, A.K. (1966) Size distribution, composition and growth kinetics of garnet crystals of some metamorphic rocks from west of Ireland. Quarterly Journal of the Geological Society of London, 122, 29-44.

Jones, K.A., Morgan, G.J., and Galwey, A.K. (1972) The significance of the size distribution function of crystals formed in metamorphic reactions. Chemical Geology, 9, 137-143.
Kerrick, D.M., Lasaga, A.C., and Raeburn, S.P. (1991) Kinetics of heterogeneous reactions. In D.M. Kerrick, Ed., Contact Metamorphism, 26, p. 583-672. Mineralogical Society of America, Washington, D. C.
Kretz, R. (1966) Grain-size distribution for certain metamorphic minerals in relation to nucleation and growth. Journal of Geology, 74, 147-173.
Kretz, R. (1969) On the spatial distribution of crystals in rocks. Lithos, 2, 39-66.
Kretz, R. (1973) Kinetics of the crystallization of garnet at two localities near Yellowknife. Canadian Mineralogist, 12, 1-20.
Kretz, R. (1974) Some models for the rate of crystallization of garnet in metamorphic rocks. Lithos, 7, 123-131.
Kretz, R. (1993) A garnet population in Yellowknife schist, Canada. Journal of Metamorphic Geology, 11, 101-120.
Lang, H.M., and Dunn, G.R. (1990) Sequential porphyroblast growth during deformation in a low-pressure metamorphic terrain, Orrs Island-Harpswell Neck, Maine. Journal of Metamorphic Geology, 8, 199-216.
Lasaga, A.C., and Kirkpatrick, R.J. (1981) Kinetics of Geochemical Processes, 398 p. Mineralogical Society of America, Washington, D. C.
Miyazaki, K. (1991) Ostwald ripening of garnet in high P/T metamorphic rocks. Contributions to Mineralogy and Petrology, 108, 118-128.
Prior, D.J., Boyle, A.P., Brenker, F., Harte, B., Speiss, R., Weber, U., and Wheeler, J. (1998) The hidden life of garnet. EOS (Transactions of the American Geophysical Union), 79, S356.
Raeburn, S.P. (1996) New methods in quantitative metamorphic petrology: 1. In situ determinations of iron valence in minerals; 2. The application of 3-D textural analysis to the study of crystallization kinetics. Ph. D. dissertation, Pennsylvania State University, University Park, PA.
Rasband, W. (1997) NIH Image. http://rsb.info.nih.gov/nih-image/.
Spear, F.S., Kohn, M.J., Florence, F., and Menard, T. (1990) A model for garnet and plagioclase growth in pelitic schists: Implications for thermobarometry and P-T path determinations. Journal of Metamorphic Geology, 8, 683-696.
Spear, F.S., and Menard, T. (1989) Program GIBBS: A generalized Gibbs method algorithm. American Mineralogist, 74, 942-943.

Table 1. Layer thicknesses (μm) for analyzed samples

Layer	96-1	96-2
1	0	0
2	30	41
3	29	30
4	37	39
5	25	19
6	44	34
7	72	62
8	54	45
9	56	53
10	49	42
Garnet diameter range (μm)	50-750	50-750

Table 2. Representative electron microprobe analyses of minerals from samples 96-1 and 96-2

Sample	96-1	96-1	96-2	96-2
Mineral	Garnet 1 core	Garnet 5 rim	Garnet 2 core	Garnet 3 rim
SiO_2	36.71	37.03	37.43	36.90
Al_2O_3	21.34	21.26	21.40	21.24
MgO	0.80	1.46	0.66	1.66
FeO	20.48	28.80	19.12	31.57
MnO	17.91	10.04	20.56	8.11
CaO	3.09	1.96	2.28	1.73
Total	100.60	100.57	101.65	101.39
		Cations per 12 oxygens		
Si	2.969	2.991	2.998	2.967
Al	2.035	2.025	2.021	2.013
Mg	0.096	0.176	0.079	0.199
Fe^{2+}	1.385	1.946	1.281	2.123
Mn	1.227	0.687	1.395	0.552
Ca	0.268	0.170	0.196	0.149
Fe/Fe+Mg	0.935	0.917	0.942	0.914
Pyrope	0.032	0.059	0.027	0.066
Almandine	0.465	0.653	0.434	0.702
Spessartine	0.412	0.231	0.473	0.183
Grossular	0.090	0.057	0.066	0.049

Table 2, continued

Sample	96-1	96-1	96-2	96-2
Mineral	Plagioclase 45 core	Plagioclase 49 rim	Plagioclase 28 core	Plagioclase 27 rim
SiO_2	63.06	66.12	63.32	67.13
Al_2O_3	23.51	20.85	23.12	20.56
CaO	4.96	1.63	4.88	1.48
Na_2O	9.45	11.11	9.26	11.72
K_2O	0.07	0.11	0.07	0.04
Total	101.21	100.12	100.79	101.01
		Cations per 8 oxygens		
Si	2.767	2.907	2.785	2.924
Al	1.216	1.081	1.199	1.056
Ca	0.233	0.077	0.230	0.069
Na	0.804	0.947	0.790	0.990
K	0.004	0.006	0.004	0.002
An	0.224	0.075	0.225	0.065
Ab	0.772	0.919	0.771	0.933
Or	0.004	0.006	0.004	0.002

Table 2, continued

Sample	96-1	96-2	96-1	96-2
Mineral	Muscovite 44	Muscovite 22	Biotite 35	Biotite 17
SiO_2	46.64	45.66	34.94	35.89
Al_2O_3	33.70	35.35	18.90	18.98
TiO_2	0.25	0.29	1.31	1.36
MgO	0.92	0.52	9.49	9.65
FeO	1.51	1.45	20.53	21.84
MnO	0.02	0.00	0.21	0.25
CaO	0.00	0.00	0.01	0.07
Na_2O	0.50	0.66	0.07	0.12
K_2O	10.22	9.82	8.58	8.19
Total	93.75	93.75	94.04	96.35
		Cations per 22 oxygens		
Si	6.299	6.156	5.401	5.420
Al^{iv}	1.701	1.844	2.599	2.580
Al_{total}	5.365	5.62	3.444	3.379
Al^{vi}	3.664	3.776	0.845	0.799
Ti	0.025	0.029	0.152	0.155
Mg	0.185	0.105	2.186	2.173
Fe^{2+}	0.170	0.164	2.654	2.758
Mn	0.002	0.000	0.028	0.032
∑Oct	4.046	4.074	5.865	5.917
Ca	0.000	0.000	0.001	0.012
Na	0.132	0.173	0.022	0.034
K	1.761	1.689	1.693	1.578
∑(A)	1.893	1.862	1.716	1.624
Fe/Fe+Mg	0.479	0.610	0.548	0.559

Table 2, continued

Sample	96-1	96-2
Mineral	Chlorite 37	Chlorite 19
SiO_2	25.42	25.02
Al_2O_3	22.72	22.06
TiO_2	0.06	0.02
MgO	12.91	13.38
FeO	26.25	28.06
MnO	0.43	0.48
Total	87.77	89.02
	Cations per 28 oxygens	
Si	5.365	5.272
Al	5.654	5.480
Ti	0.009	0.003
Mg	4.061	4.202
Fe^{2+}	4.634	4.944
Mn	0.076	0.085
Fe/Fe+Mg	0.533	0.541

Table 3. Initial conditions for simulations of Mn zoning in garnet

Phase	Initial mode (cm^3)	Composition
Quartz	0.2	$X_{SiO_2} = 1$
Fluid	0.0	$X_{H_2O} = 1$
Muscovite	0.3	$X_{ms} = 0.84$; $X_{celadonite} = 0.07$; $X_{Fe\text{-}celadonite} = 0.09$
Biotite	0.2	$X_{Mg} = 0.30$; $X_{Fe} = 0.68$; $X_{Mn} = 0.02$
Chlorite	0.3	$X_{Mg} = 0.34$; $X_{Fe} = 0.63$; $X_{Mn} = 0.03$
Garnet	0.0	$X_{Mg} = 0.10$; $X_{Fe} = 0.60$; $X_{Mn} = 0.30$

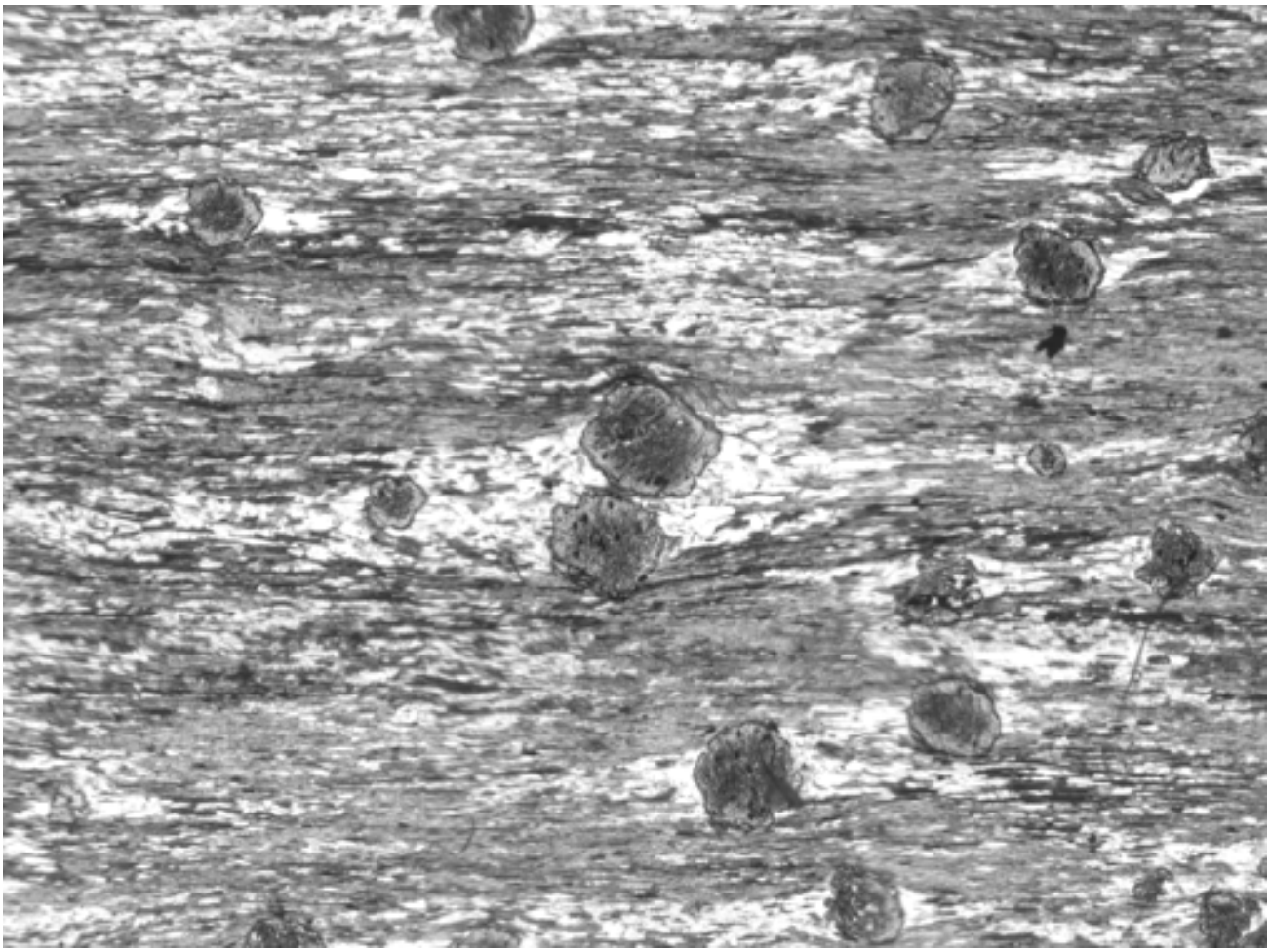

Figure 1. Photomicrograph of sample 96-1. Section is cut perpendicular to foliation and parallel to lineation. Width of field is 6 mm. Note pressure shadows around garnet, which are demonstrated to be symmetrical discs in sections cut parallel to foliation (Fig. 3).

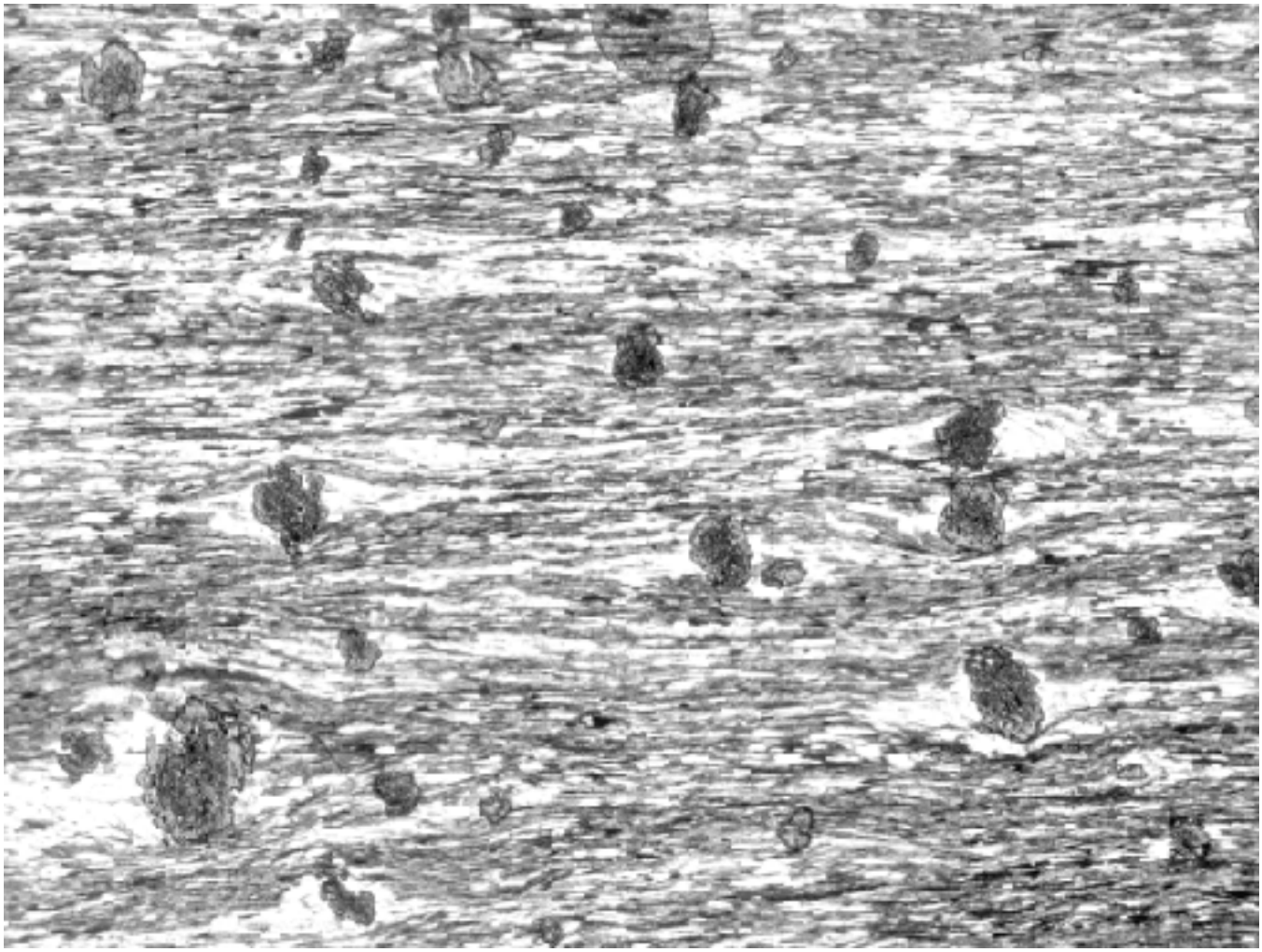

Figure 2. Photomicrograph of sample 96-2. Section is cut perpendicular to foliation and parallel to lineation. Width of field is 6 mm.

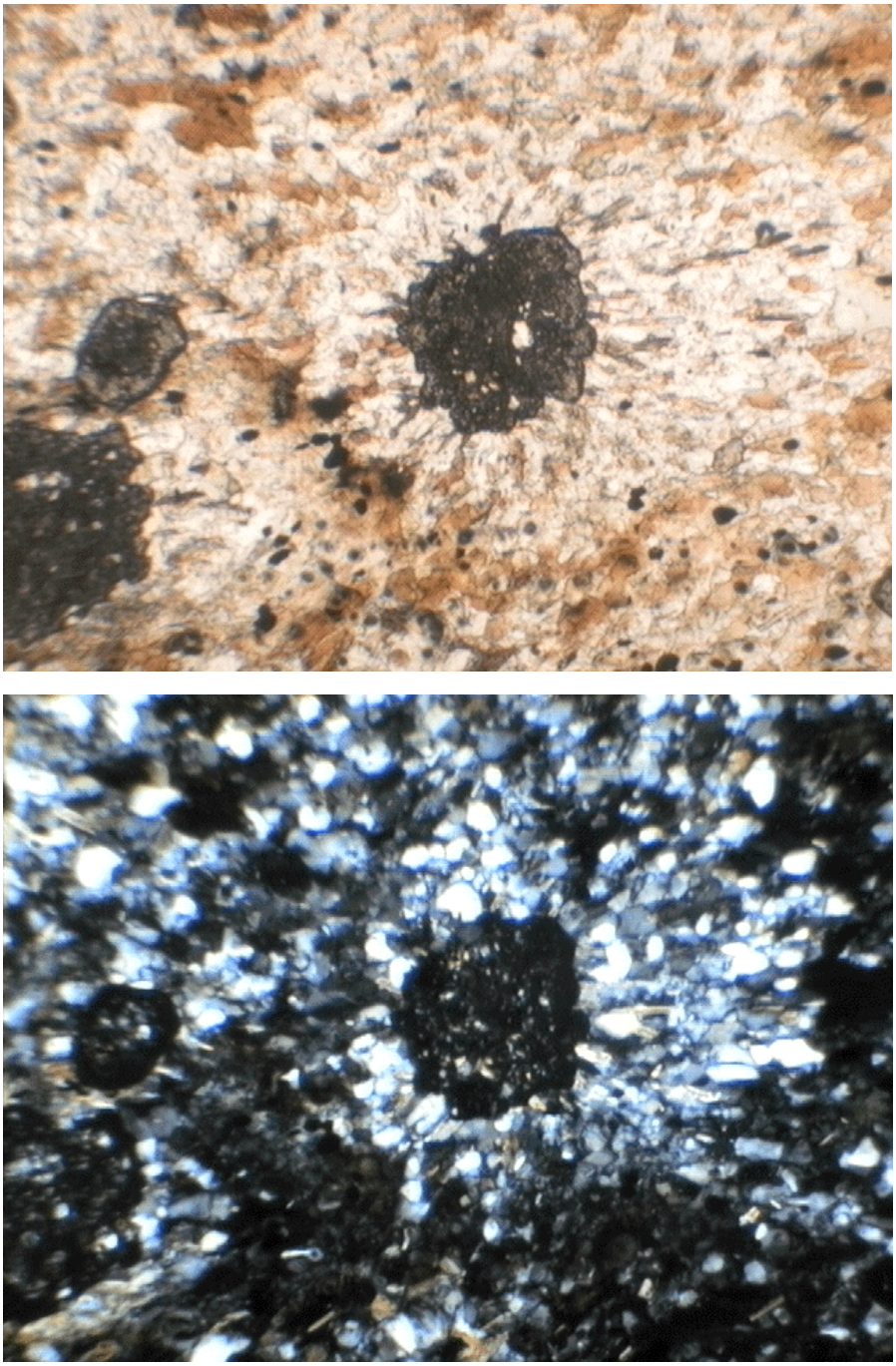

Figure 3. Photomicrograph of sample 96-1 cut parallel to foliation showing a roughly circular pressure shadow around garnet. Pale green crystals are chlorite; small blades of chlorite form a radial array in the pressure shadow around garnet. Brown crystals are biotite, colorless crystals are quartz and plagioclase, black crystals are ilmenite. Width of field is 2 mm.

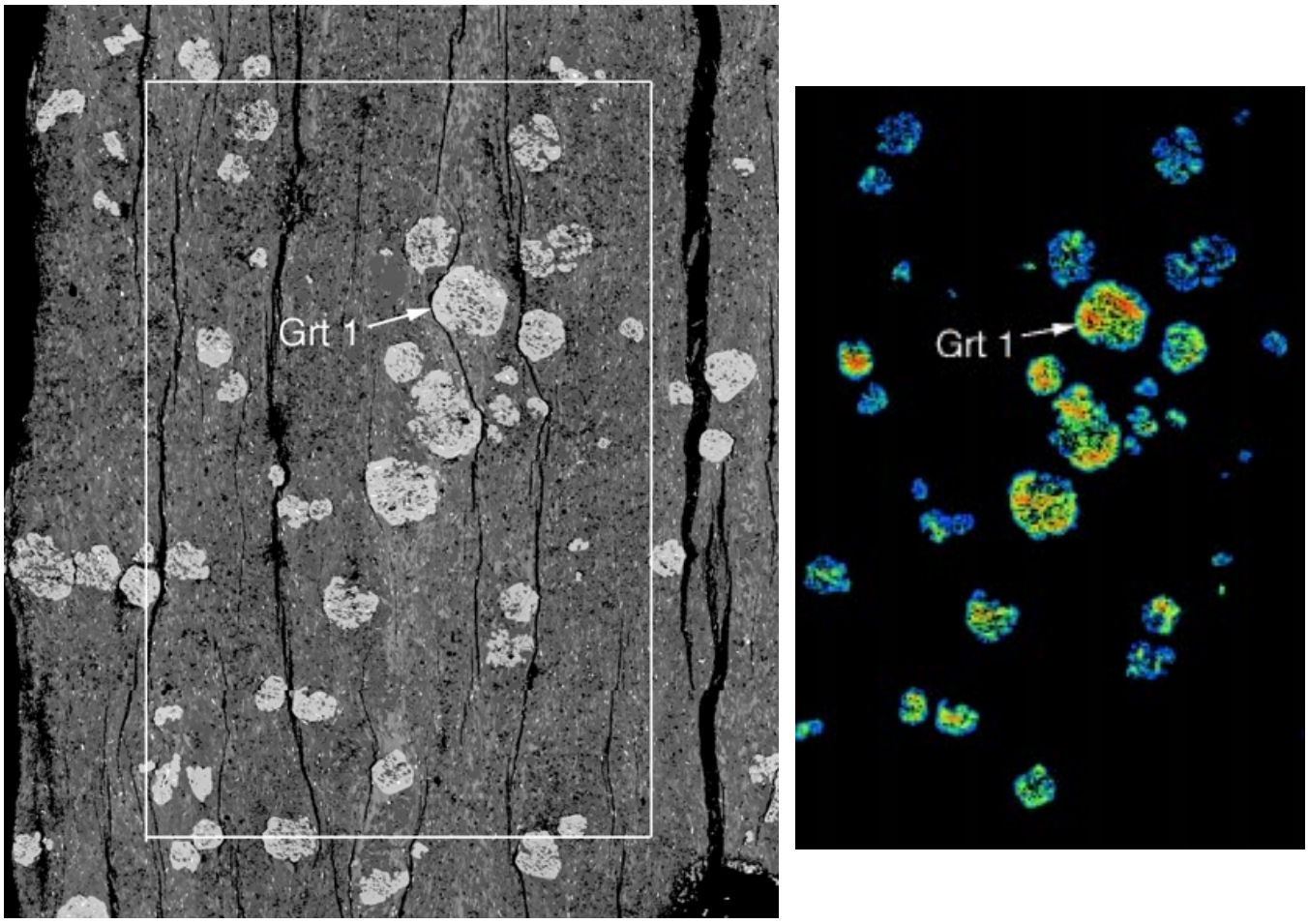

Figure 4. Representative images layer 9, sample 96-1.
(a) BSE mosaic comprised of 12 tiles (3x4) collected at 40x magnification (3.3 x 3.3 mm) with a resolution of 5 μm/pixel. Large box shows area of (b) and has dimensions 5 x 7 mm. Arrow shows location of garnet 1 (Figs. 8a, 9, 10, 11).
(b) Mn X-ray map mosaic of a 5 x 7.5 mm area showing composition zoning in garnet. Warm colors are higher values. Black regions are garnet-free matrix. Resolution = 5 μm/pixel.
(Larger GIF image available for download)

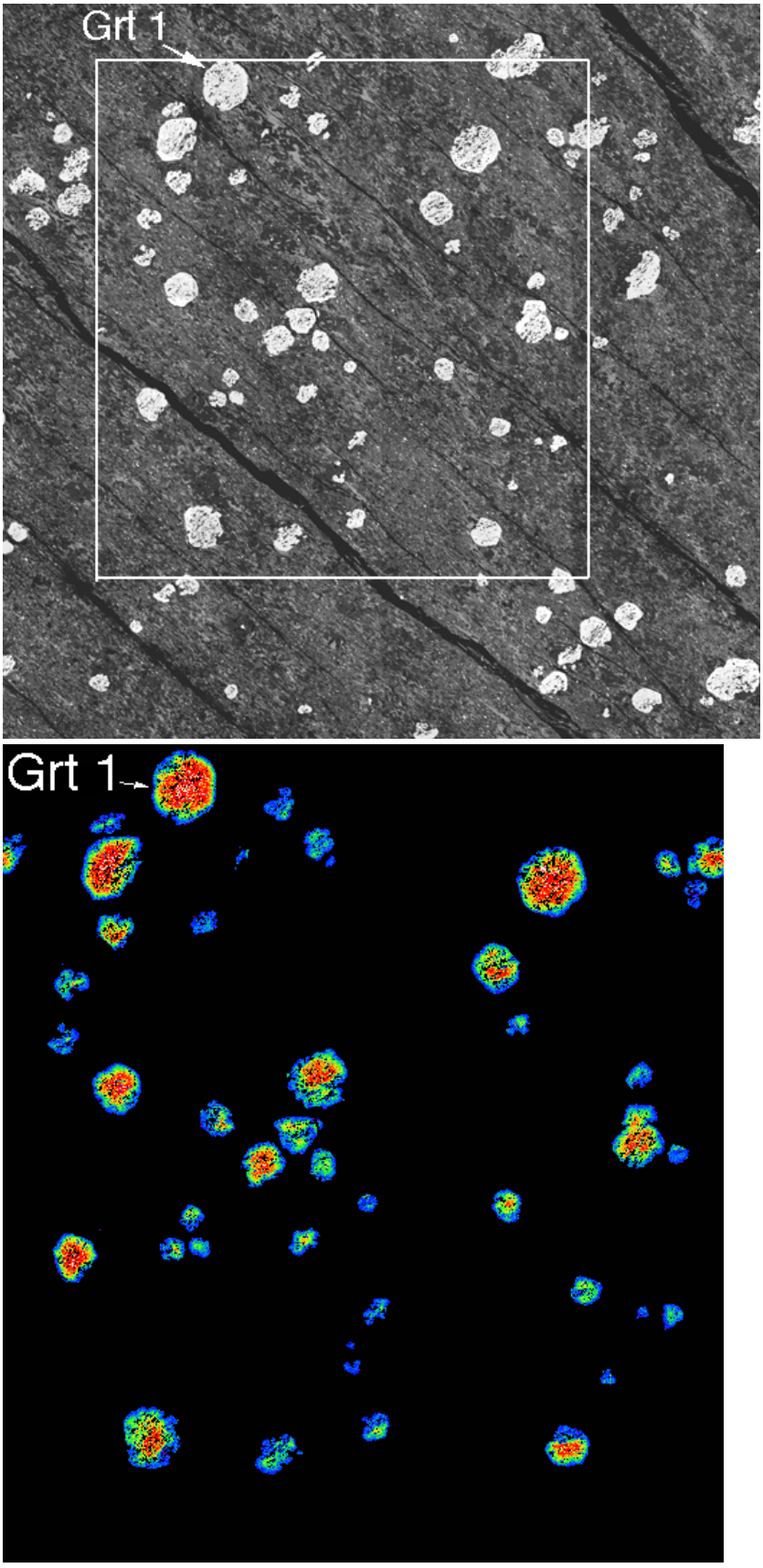

Figure 5. Representative images of layer 4, sample 96-2.

(a) BSE mosaic comprised of 20 tiles (4x5) collected at 40x magnification(3.3 x 3.3 mm) with a resolution of 5 μm/pixel. Large box shows area of (b) and has dimensions of 7.5 x 8.5 mm. Arrow shows location of garnet1 (Fig. 8b).

(b) Mn X-ray map mosaic of a 7.5 x 8.5 mm area showing composition zoning in garnet. Warm colors are higher values. Black regions are garnet-free matrix. Resolution = 5 μm/pixel in the original map.
(Larger GIF image available for download)

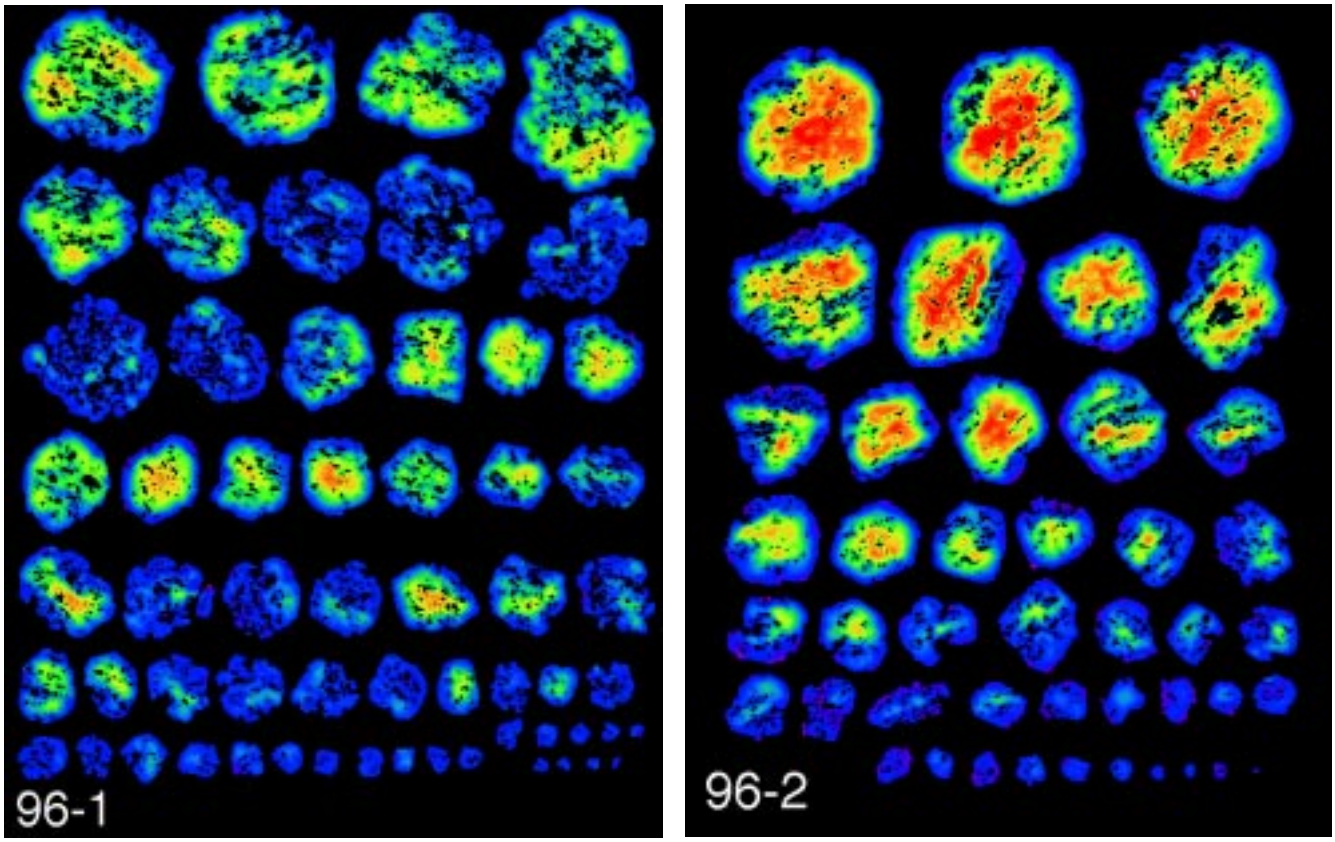

Figure 6. X-ray maps showing distribution of Mn in center cuts through garnets from samples 96-1 (a) and 96-2 (b) ordered according to size. Note the strong correlation of garnet core composition with size and the consistency of composition on the rims of all crystals from the same sample. Warm colors are higher values. (Larger GIF images available for download)

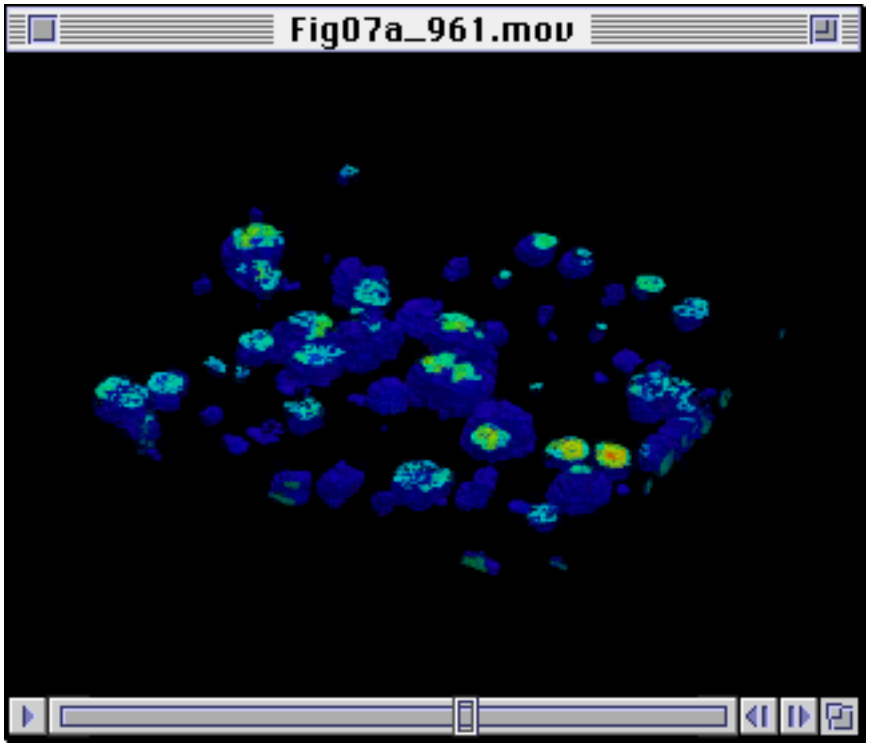

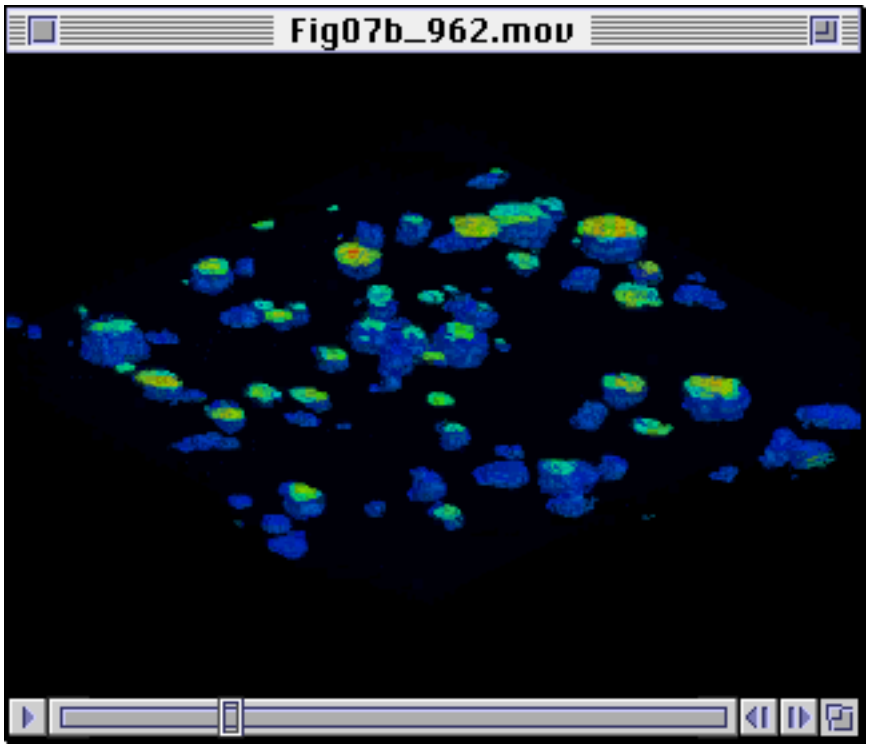

Figure 7. Three-dimensional constructions (Quicktime movies) showing positions of garnets. (a) Sample 96-1 (b) Sample 96-2. [Ed's. note: Quicktime movies may open in a browser window behind the Acrobat window. If browser timeout occurs, try the "Reload" button.]

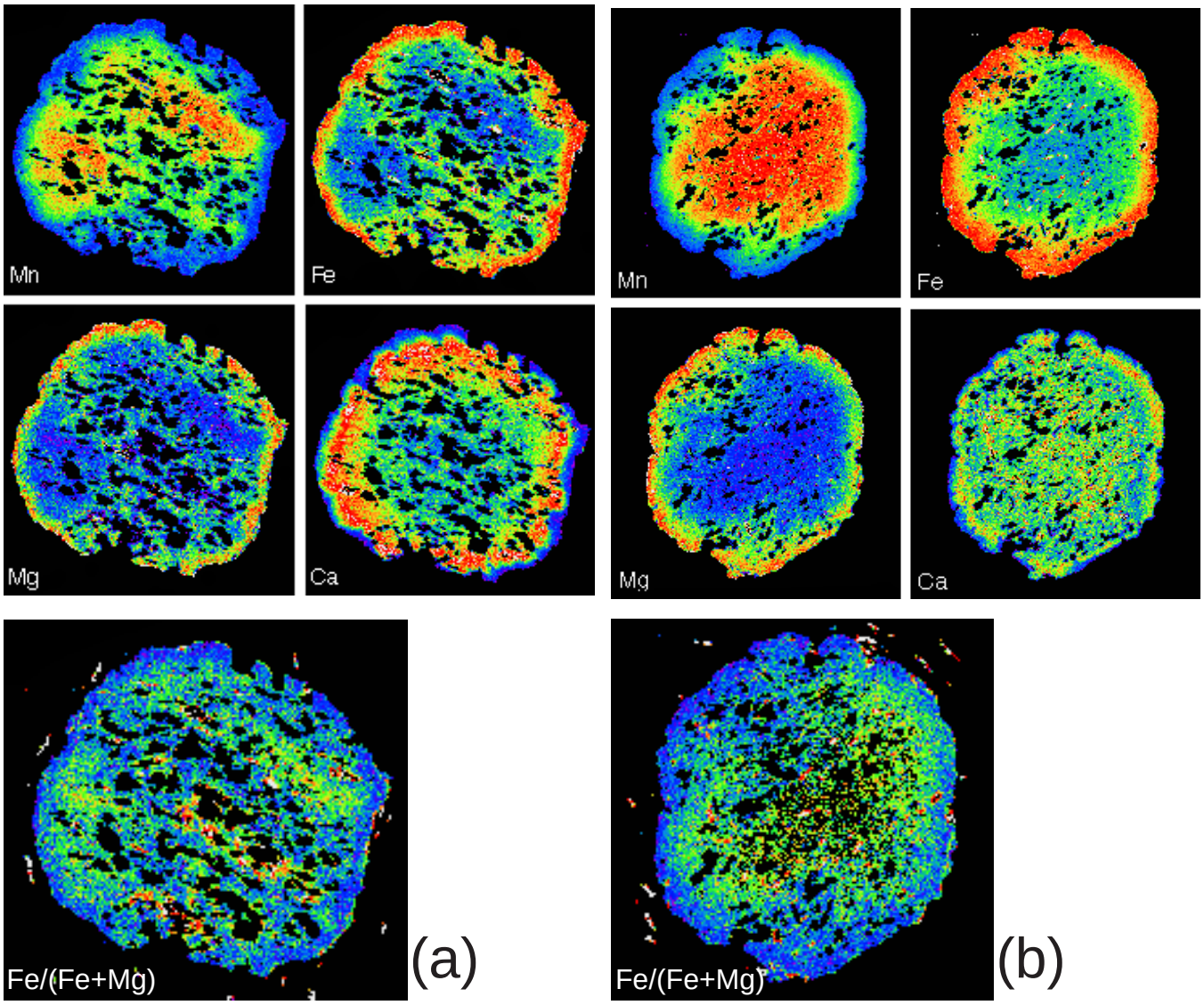

Figure 8. X-ray composition maps showing 2-dimensional compositional zoning in the largest garnet from samples (a) 96-1 and (b) 96-2 (see Figs. 4 and 5). Warm colors are higher values. Microprobe operating conditions: 200 na, 20 ms/pixel. Resolution = 5 μm/pixel. Garnet diameter = 750 μm.

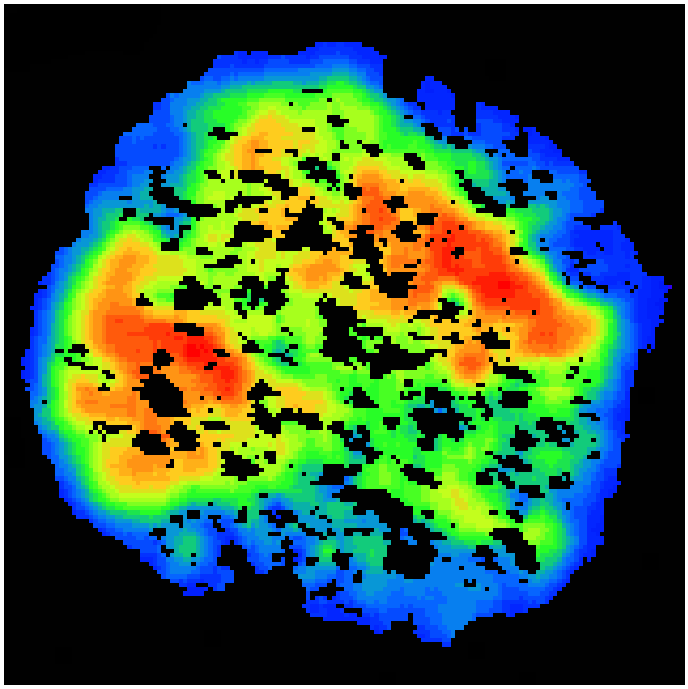

Figure 9. Mn X-ray composition map, sample 96-1, layer 9, garnet 1. Smoothing kernel (7x7) with edge recognition has been applied to this image. Note the amoeba-like shapes of the Mn zoning, especially around quartz inclusions. Garnet diameter = 750 μm. Warm colors are higher values.

(a) 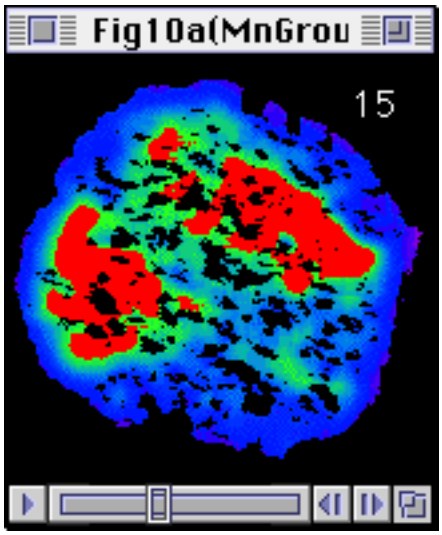

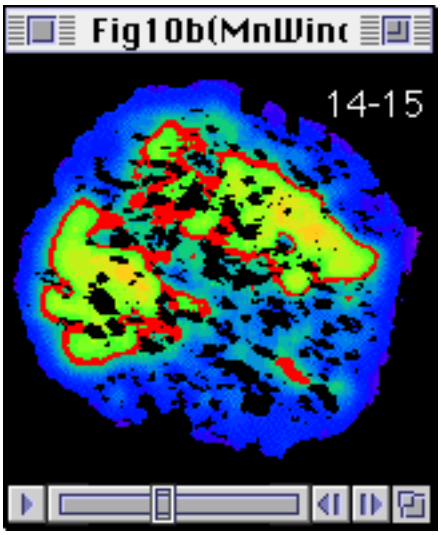

(b)

Figure 10. Quicktime movies showing Mn growth history, sample 96-1, layer 9, garnet 1.
(a) Red shows cumulative Mn growth. Number (e.g. 15) represents the lower MnO concentration (weight per cent).
(b) Red shows incremental Mn growth. Numbers give the lower and upper bounds of the MnO concentration window. Garnet diameter = 750 μm. Note the appearance of new nuclei as garnet grew.
[Ed's. note: Quicktime movies may open in a browser window behind the Acrobat window. If browser timeout occurs, try the "Reload" button.]

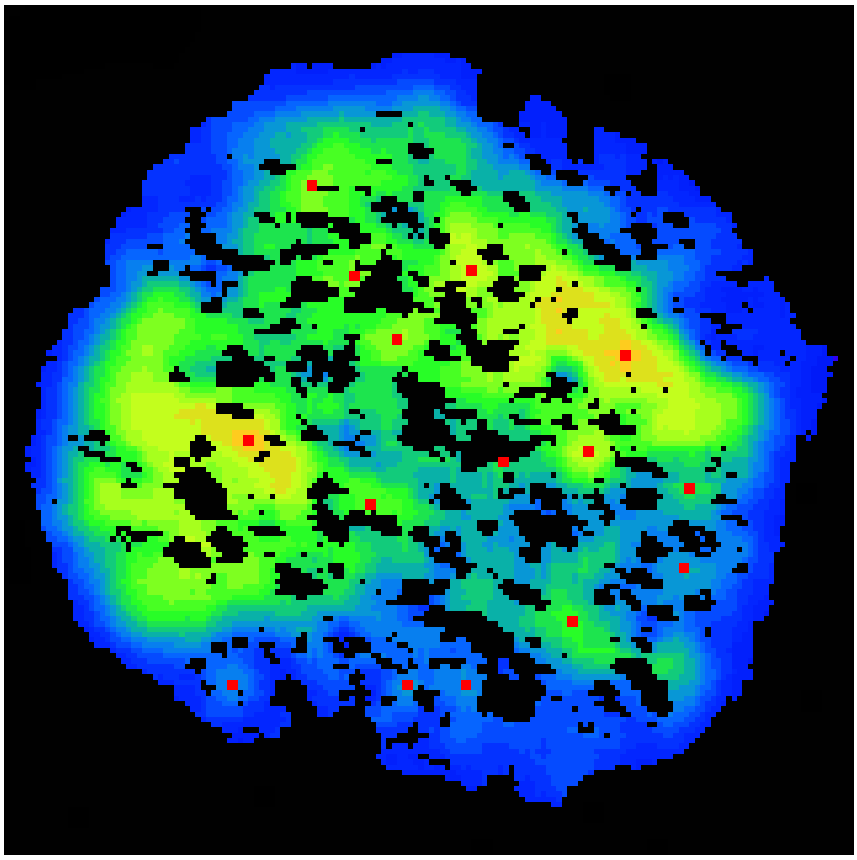

Figure 11. Distribution of distinct garnet nuclei (shown as red squares) that appear during the growth of garnet 1, layer 9, sample 96-1. Warm colors are higher values. Garnet diameter = 750 μm.

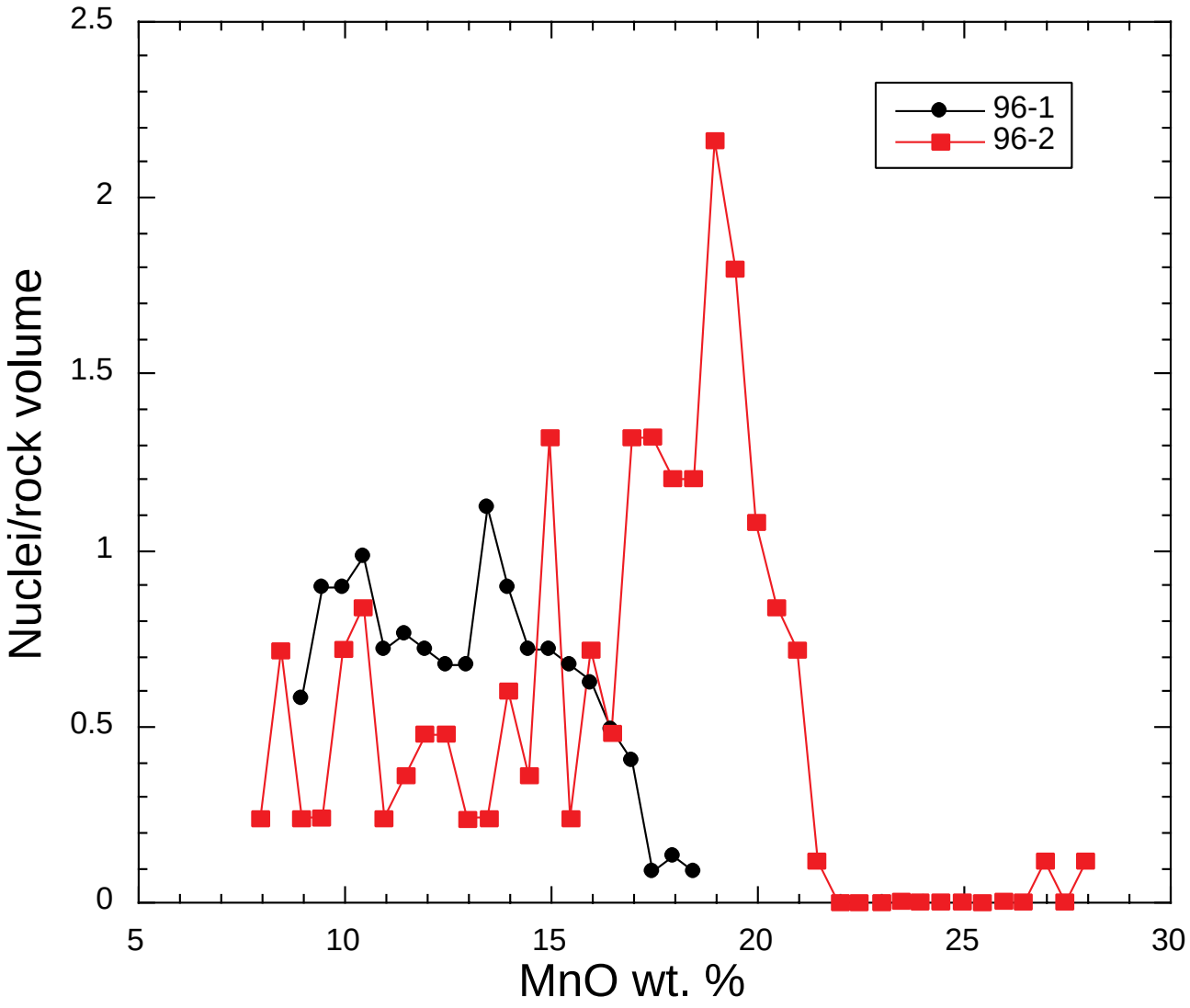

Figure 12. Plot of number of nuclei observed as a function of MnO concentration in garnet normalized to the volume of rock sampled. Sample 96-1 has 59 garnets; sample 96-2 has 44 garnets.

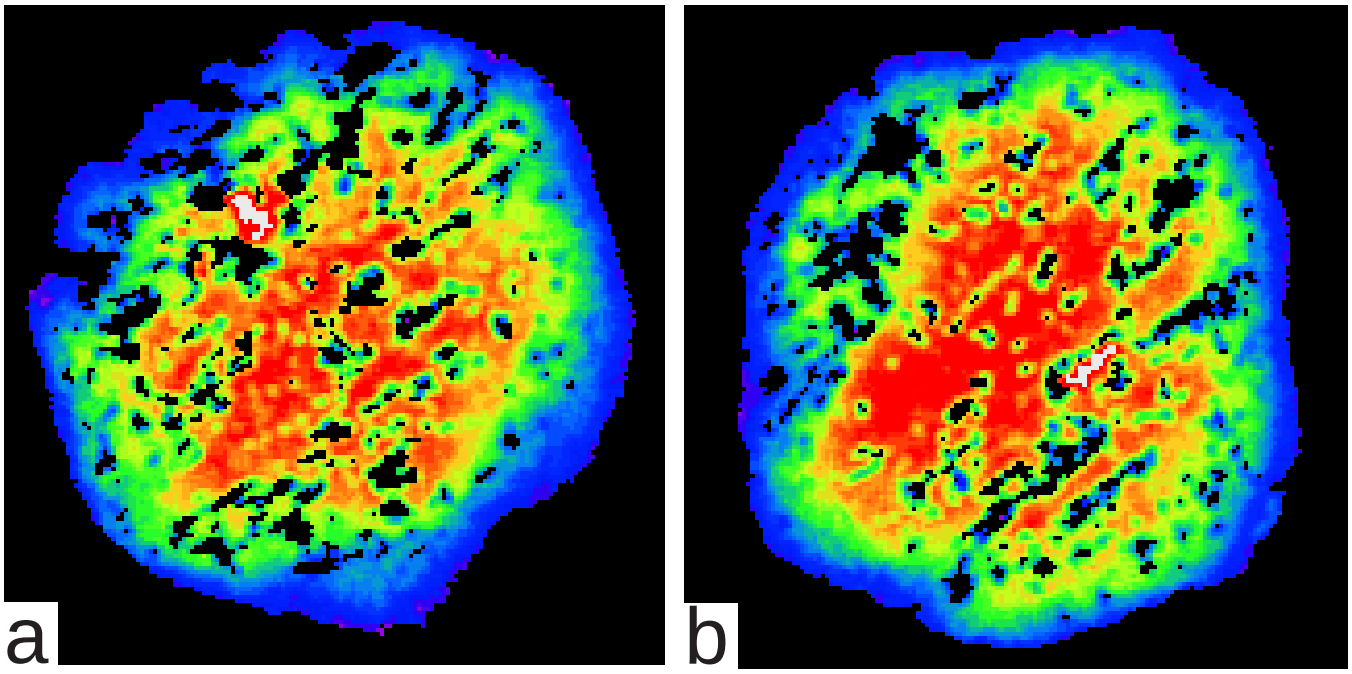

Figure 13. Mn X-ray maps of two large garnets from sample 96-2 showing Mn-rich regions (white areas = 5 wt. % greater than adjacent garnet), which are interpreted to be detrital grains. Note that the Mn-rich domains do not lie in the core of the crystals. Warm colors are higher values.

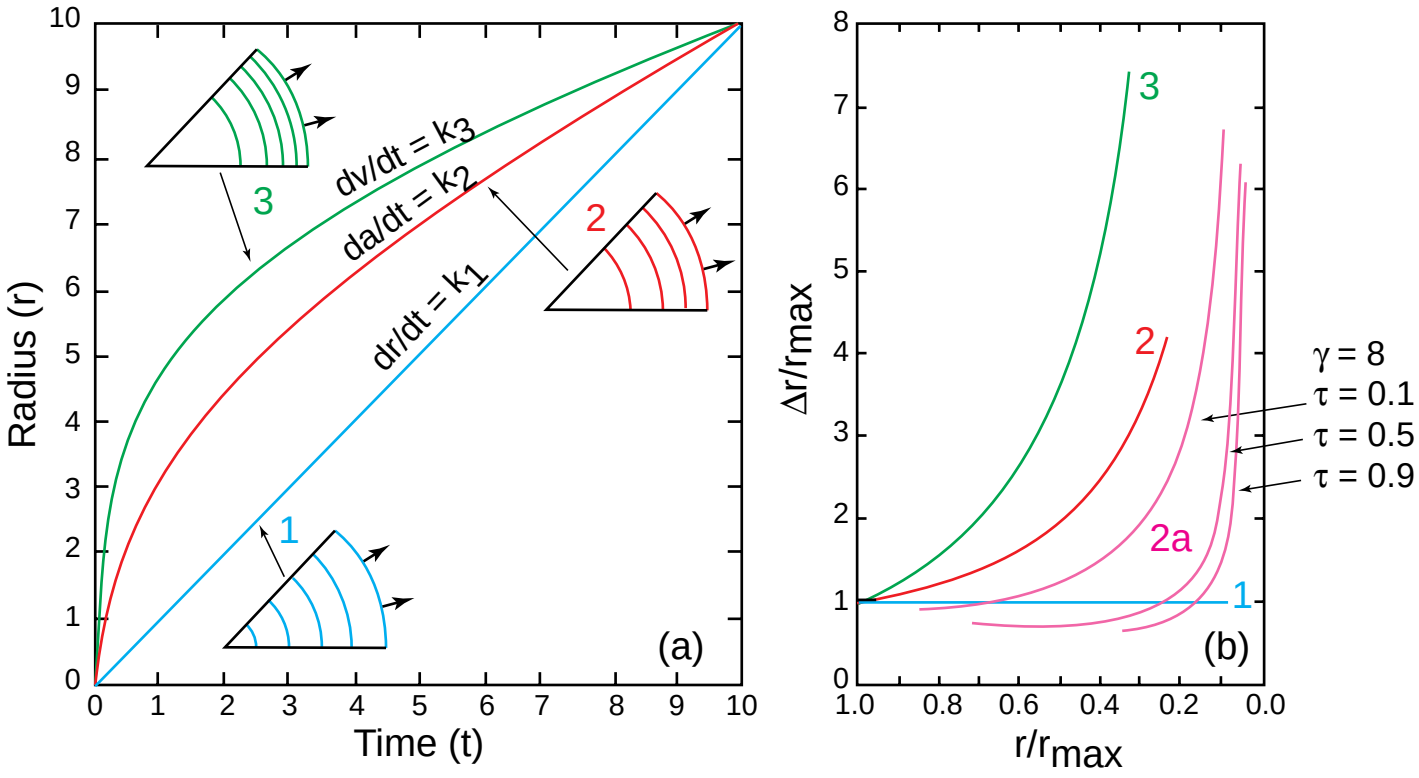

Figure 14. Theoretical garnet growth models.

(a) Plot of radius versus time for three models of garnet growth (from Kretz, 1974):
Case 1: dr/dt = constant; all garnets grow at same rate regardless of size and there is equal spacing between growth rings;
Case 2: da/dt = constant; small garnets grow faster than large garnets and growth rings get closer together towards the rim;
Case 3: dv/dt = constant; small garnets grow faster than large garnets and growth rings get closer together towards the rim.

(b) Normalized radius-rate plot for three models of garnet growth. Curves 1, 2 and 3 are from Kretz (1974). Curves 2a are radius-rate plots for the thermally accelerated diffusive growth model of Carlson (1989) with $\gamma = 8$ (nondimensional temperature increase) and three values of τ (nondimensionalized time since first garnet nucleated). Note that in this model small garnets first grow faster than the largest garnet (near the core) and later grow more slowly than the largest garnet (towards the rim).

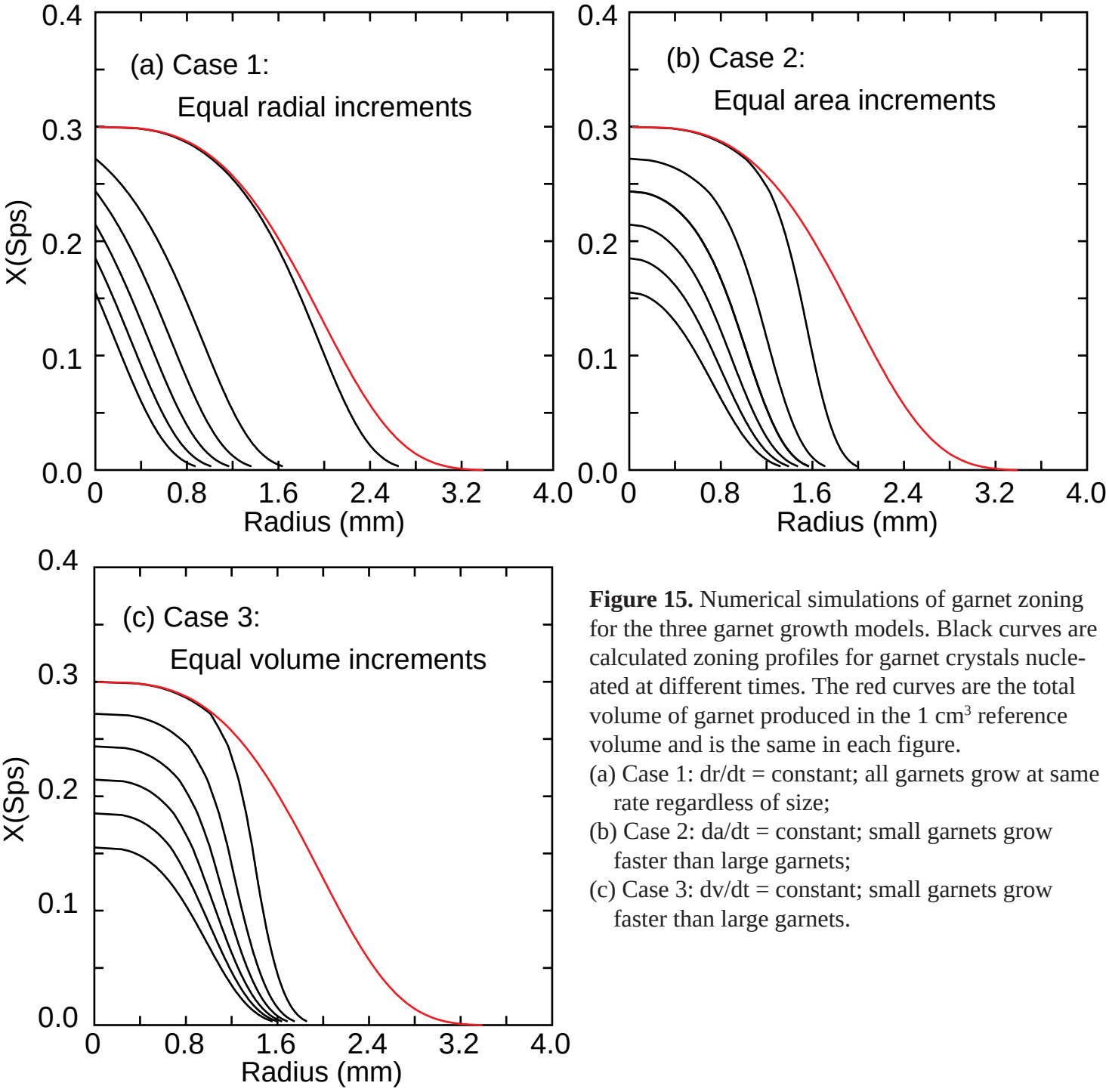

Figure 15. Numerical simulations of garnet zoning for the three garnet growth models. Black curves are calculated zoning profiles for garnet crystals nucleated at different times. The red curves are the total volume of garnet produced in the 1 cm^3 reference volume and is the same in each figure.
(a) Case 1: dr/dt = constant; all garnets grow at same rate regardless of size;
(b) Case 2: da/dt = constant; small garnets grow faster than large garnets;
(c) Case 3: dv/dt = constant; small garnets grow faster than large garnets.

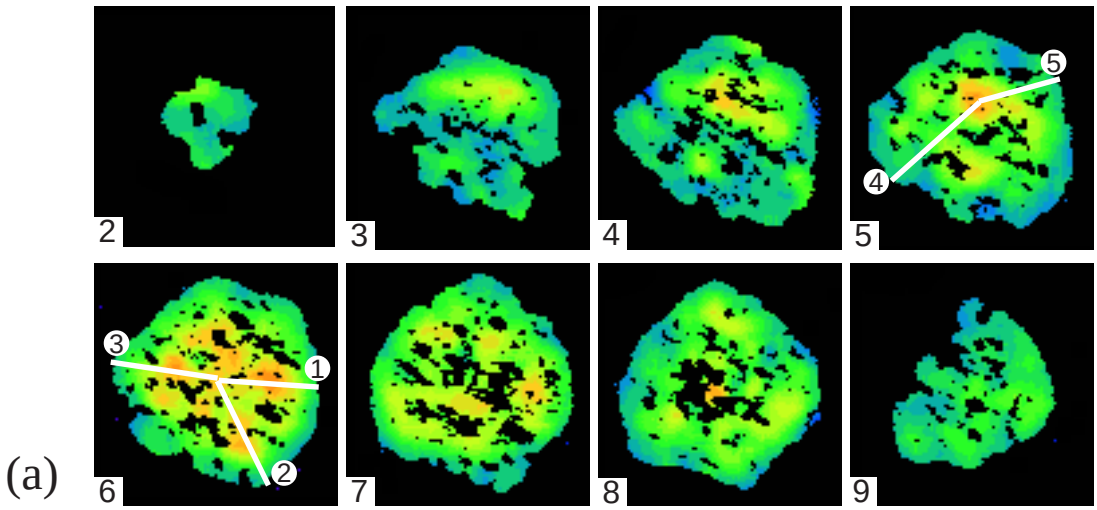

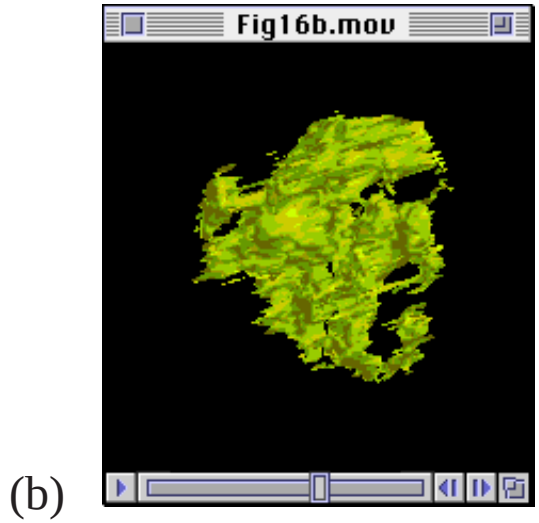

Figure 16. Mn X-ray composition maps of garnet 22, sample 96-1.
(a) X-ray maps through each of eight layers White lines show locations of 5 line traverses (Fig. 17b).
(b) Quicktime movie showing 3-dimensional animation of garnet zoning using Mn as a time line. Note irregular outline of garnet crystal (ameoba-shaped) and cavities, which are quartz grains that have not totally dissolved. [Ed's. note: Quicktime movies may open in a browser window behind the Acrobat window. If browser timeout occurs, try the "Reload" button.]

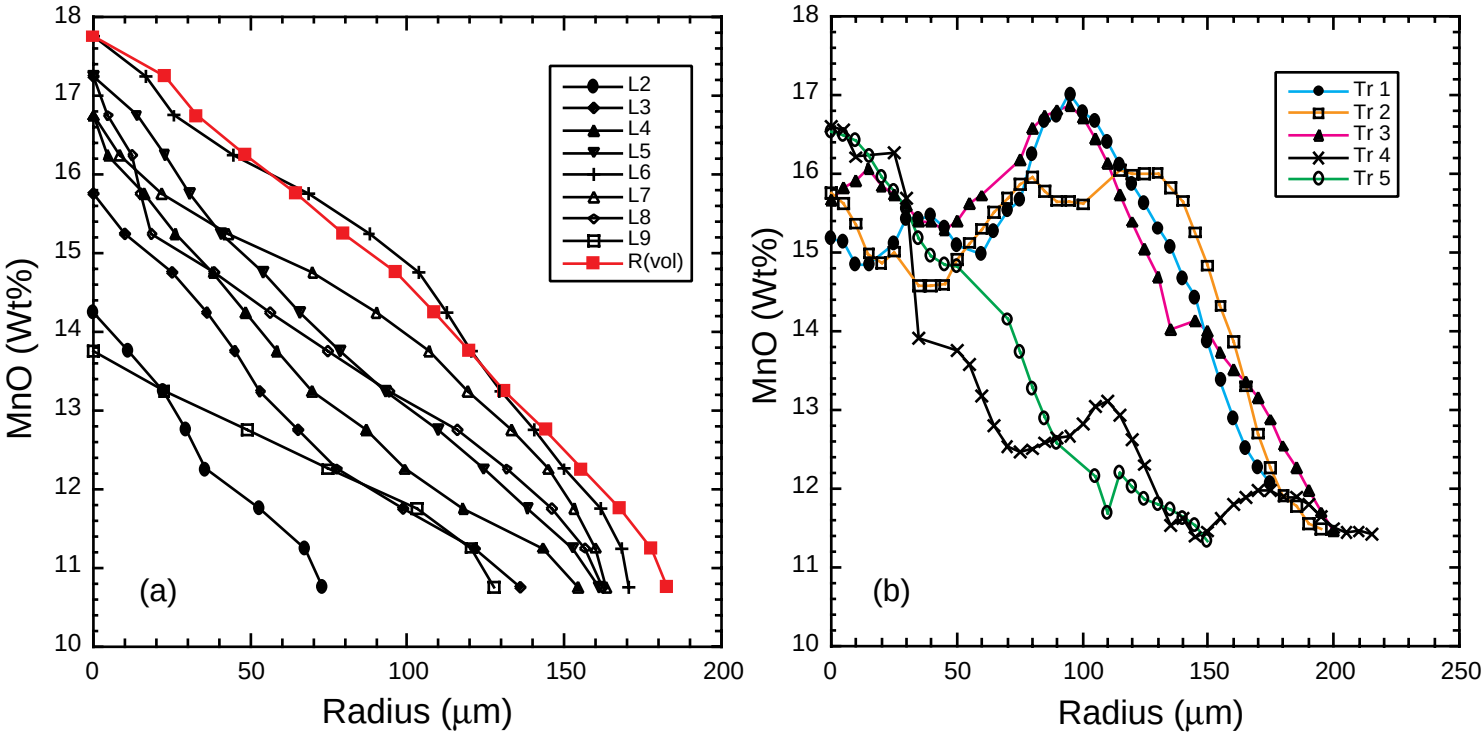

Figure 17. Plots showing MnO concentration (wt. %) versus apparent radius for three methods of calculating Mn zoning from X-ray images. (a) Computed MnO concentration (wt. %) versus radius from measuring areas on X-ray maps for all eight layers (black curves and symbols) and from summing total volume over all layers (red curve).
(b) Measured MnO concentration versus radius along five line traverses (see Fig. 16a for locations of traverses).

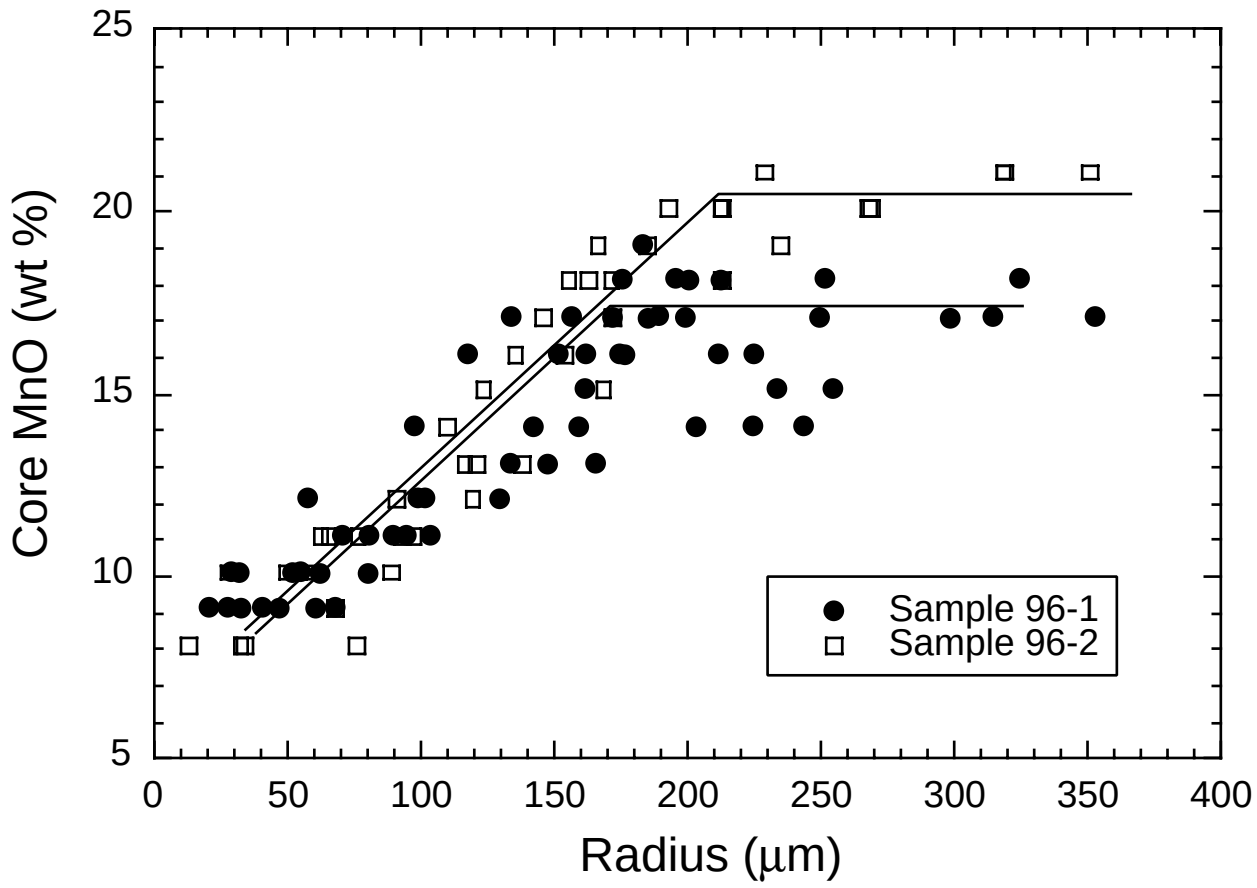

Figure 18. Plot of the concentration of MnO (wt. %) in garnet cores versus garnet radius. Lines are drawn by inspection to show trends of data.

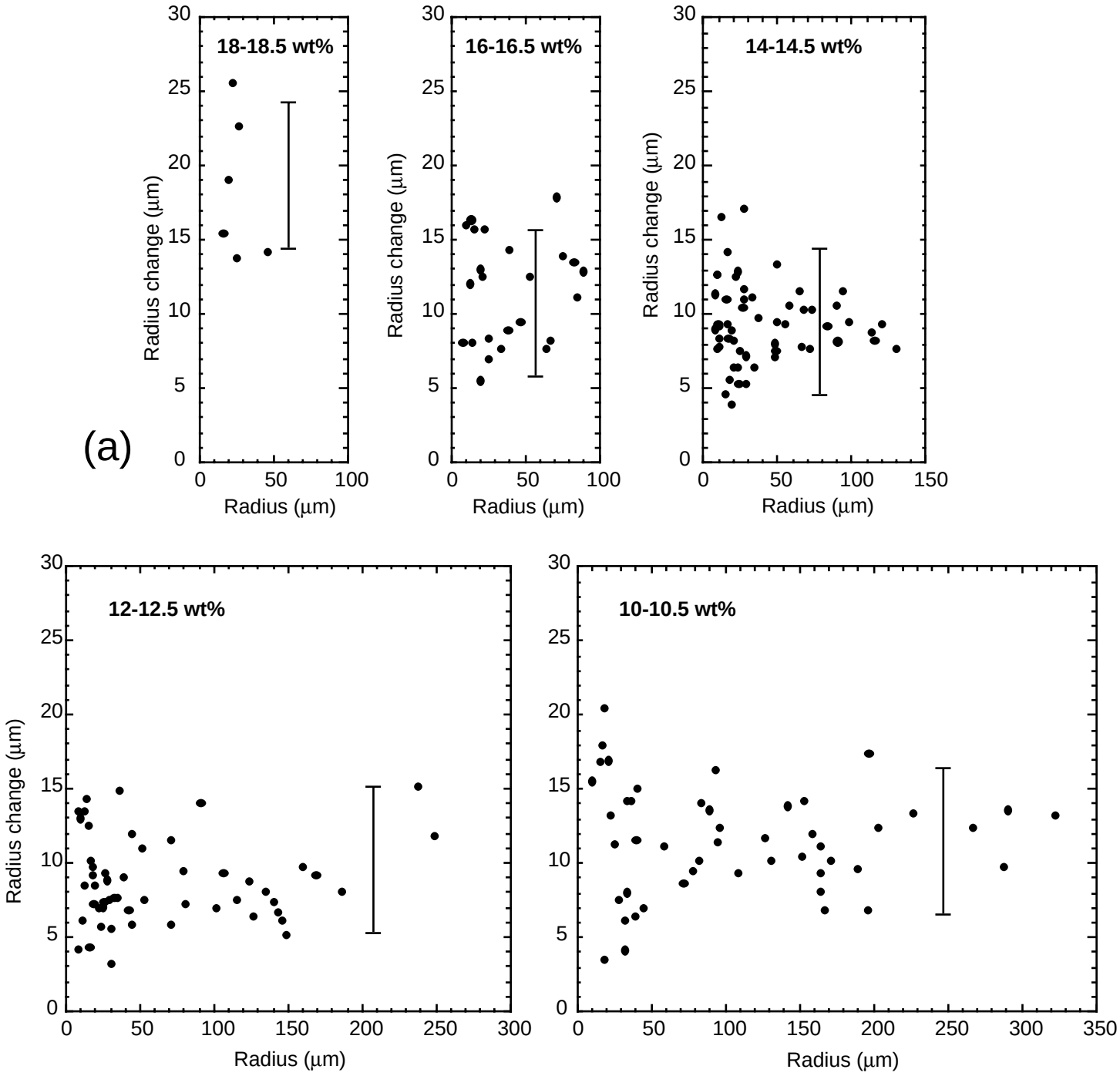

Figure 19. Plot of radial change versus radius (radius-rate plot) for Mn composition windows. Error bars shown are ±1 pixel (= 5 μm).
(a) Sample 96-1.
(b) Sample 96-2 (following page).

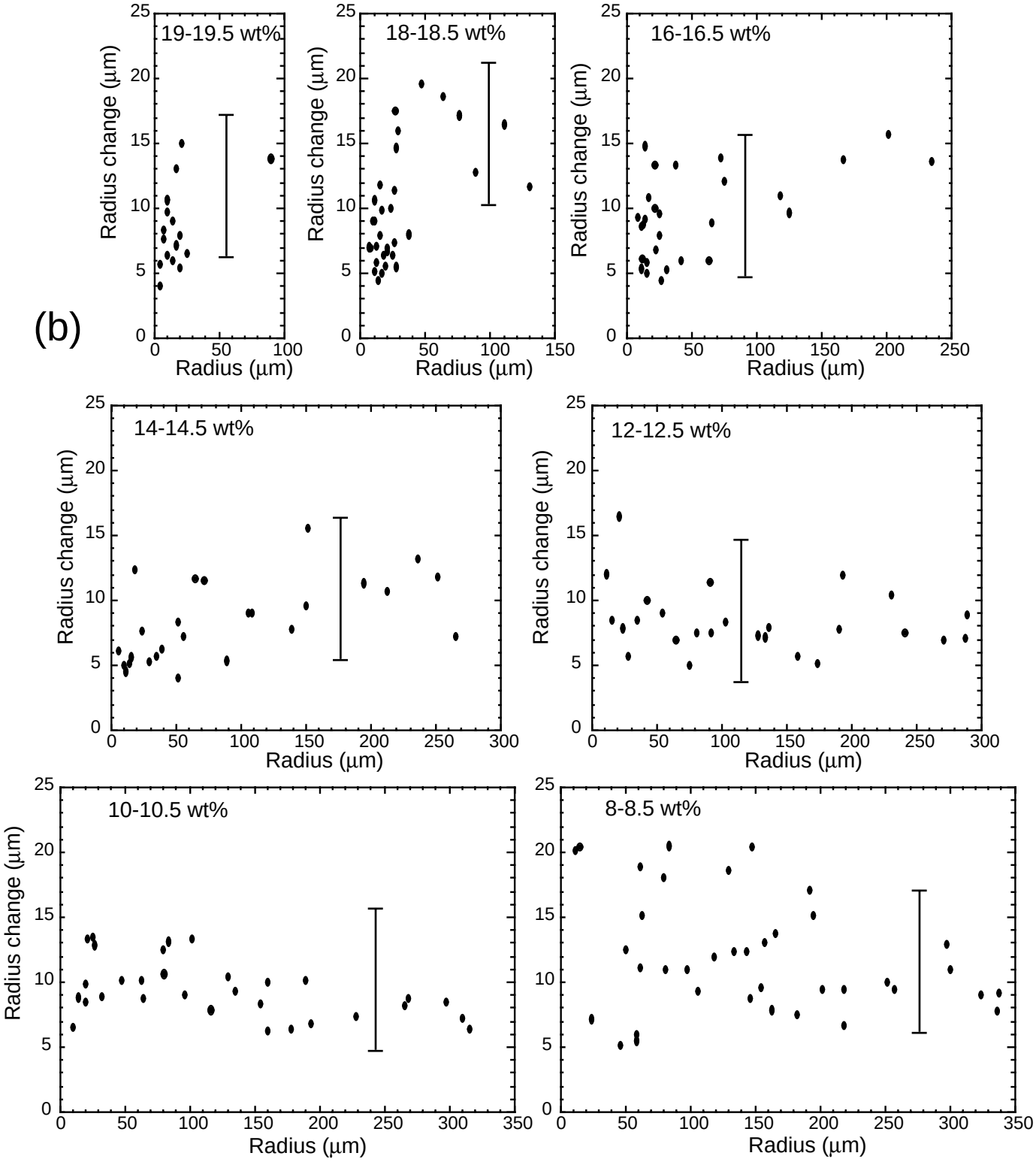

Figure 19. continued.
(b) Sample 96-2.

Appendix

Larger GIF images of Figures 4b, 5b, 6a, and 6b are available. Press here to obtain copies.